REPORT

Drainage Åknes

COUPLED HYDRO-MECHANICAL STABILITY ANALYSIS OF ÅKNES ROCK SLOPE

DOC.NO. 20180662-07-R
REV.NO. 0 / 2020-12-18

NORWEGIAN GEOTECHNICAL INSTITUTE
NGI.NO

Project

Project title:	Drainage Åknes
Document title:	Coupled hydro-mechanical stability analysis of Åknes rock slope
Document no.:	20180662-07-R
Date:	2020-12-18
Revision no. /rev. date:	0

Client

Client:	NVE
Client contact person:	Gustav Pless
Contract reference:	Research and development contract, signed 12 September 2018

for NGI

Project manager:	Kristin H. Holmøy
Prepared by:	Mahdi Shabanimashcool
Reviewed by:	Vida Kveldsvik

Summary

Stability of Åknes rock slide was assessed by coupled hydro-mechanical numerical analysis. The analysis was carried out by considering explicitly the rock joints network and the sliding planes.

Numerical analysis shows that with draining all the groundwater from the sliding surface the factor safety will improve ca. 0.5 and 4 % in the east and west flank of the slope, respectively.

Fast infilling of the backscarp due to flooding can destabilise the west flank: decreasing the factor of safety to 0.89.

It was shown that in hypothetically highest groundwater level inside the rock mass, the west flank has higher tendency of becoming unstable than the east flank.

Contents

Review and reference page

1 Introduction

This report presents results of the stability analysis of the Åknes rock slide. It considers latest updates regarding the geometry and depth of the sliding planes as well as the groundwater head on the sliding planes.

NGI has produced two reports which covers the hydrogeology of Åknes [1] and correlation of the monitoring results and geology [2]. These reports are used as the base for stability analysis in terms of input data.

In this study coupled hydromechanical analysis is used to carry out the stability analysis, meaning that not only groundwater effect on the effective normal stress is considered but also the effect of the rock mass stress on the hydraulic conductivity (water flow in the discontinuities) is considered.

2 Literature review

Several attempts have been made to assess stability of Åknes rock slide earlier.

The first stability analysis of Åknes was carried out by Eystein Grimstad in NGI [3]. The report mentions that the depth of the sliding plane is located at the depth of 15 – 45 m, with 20 m in average (based on available short boreholes in 1989 which is the upper visible sliding plane, see [2]). The unstable zone located at the elevations of 550 to 900 meters above sea level (m.a.s.l.) The report classifies the slope to east and west sections with different movement and sliding velocity. The western side is unstable even in the dry season while the east side is stable in the dry season. He used analytical technique considering the Barton-Bandis model [4] and calculated the factor of safety for a cross-section in the east side and the west side.

His calculations show that JRC (Joint Roughness Coefficient) value above 3 will lead to a factor of safety larger than 1 in the west side while JCS (Joint Compressive Strength) and residual friction angles are 118 MPa and 26º. Based on field mapping, he concluded that the best fitting value for the JRC is a number around 5.5. Later, he showed that by increasing the pore pressure over the sliding plane to 10 m the factor of safety decreases to below one for JRC = 5.5.

In [3] the geologist was aware of the uncertainties regarding the assumed depth of sliding plane. Therefore, he carried out sensitivity analysis on the depth of sliding plane by varying it from 5 to 40 m, with JRC=5.5, JCS = 118 MPa and φ_r = 26˚ kept constant. The results of the calculations show that the factor of safety decreases with depth while it is more than 1.2 for depths less than 45 m (Figure 1).

Tabell 5. Normalspenning, σ, Skjærspenning, P/A, Skjærfasthet, τ_p og sikkerhetsfaktor, F som funksjon av tykkelsen på bergmassen i tørr tilstand.

Tykkelse i m		5	10	20	30	40
σ	MPa	0,113	0,226	0,452	0,679	0,906
P/A	MPa	0,074	0,147	0,293	0,441	0,588
τ_p	MPa	0,104	0,196	0,370	0,537	0,699
F		1,40	1,33	1,26	1,22	1,19

Figure 1 Calculations from [3] which show that the factor of safety decreases with depth.

The first numerical modelling of Åknes was carried out by NGI [5]. The modelling mostly confirms the calculations carried out in [3]. The depth of sliding plane was set at ca. 25 m and it is confirmed by the numerical modelling that the factor of safety is 1.0. Later on, they showed that with increasing water head over the sliding surface (10 m) the rock mass becomes unstable (factor of safety < 1.0). The input data and sliding surface geometry is the same as in [3].

Numerical modelling by Kveldsvik et al. (2009) [6] consists of two different modelling approaches. First DDA-backward modelling is carried out. The slope was divided into different blocks based on displacements measured at the slope surface. Second, they carried out numerical modelling by UDEC. By varying fracture geometry, fracture friction and ground water conditions within reasonable limits based on site-specific data several possible models were compared. Models that were unstable to great depths were in closer agreement with shear strength parameters derived from an earlier study than models that were unstable to smaller depths. Further, it was shown that increasing ground water table is less critical for very deep slope instability than shallower instabilities.

Dynamic numerical modelling carried out by Kveldsvik et al. (2009) [7] tries to assess the stability of Åknes under earthquakes. The dynamic input was based on earthquakes with return periods of 100 and 1000 years. Models with ground water conditions derived from site investigations were analysed, as well as models with assumed ground water conditions from possible future draining of the slope. The analyses indicate that an earthquake with return period of 1000 years is likely to trigger sliding to great depth at the present ground water conditions, and that the slope will be stable if drained.

Numerical modelling carried out by Grøneng et al. (2009 and 2010) [8] and [9] aims at investigating the time dependent behaviour of Åknes rock slide. The depth of sliding plane is at 105 – 115 m. The water head is assumed in the model which is at depth of 40 – 60 m; and it sinks down to the sliding plane at the toe area. The model considers the whole unstable areas of west and east flank in 3D. The resistance of the sliding plane is

assumed to follow some percentage of intact rock (rock bridges), and surface contact which changes based on GSI value.

There are several master theses which tried to study the stability of Åknes numerically. Most of the master candidates also tried to find the depth of the sliding plane via numerical modelling and check the effect of the ground water on the stability of the slope. However, there are exceptions, such as Langeland (2014) [10] who tried to model the geometry of the sliding plane based on the data from DMS-es. In this thesis also three different scenario of ground water head was considered in the analysis, representing low, high and average measured values. The conclusions from the modelling show that the groundwater has neglectable effect on the stability of the slope in the western side. However, it mentions that there are uncertainties concerning the geometry and depth of the sliding planes plus groundwater head on the sliding planes.

In most of the references mentioned above, the depth of the sliding plane either was not considered directly or considered as far deeper / shallower than the confirmed sliding surface by DMS-es (see [2]). In addition, water head on the sliding plane was studied in detail and a comprehensive report was produced by NGI [1] which can be used in stability assessments. Therefore, the current numerical modelling has less uncertainty compared to the previous works concerning the depth and geometry of the sliding planes and the groundwater. In addition, it considers the coupled hydro-mechanical effects in the stability analysis.

3 Input data

This report is focusing on cross-sections W2 and E1 (Figure 2- Figure 4). Cross-section W2 is the only cross-section where data from the three boreholes KH-01-2012, KH-02-2017 and KH-01-2018 can be used for interpretation of sliding planes and groundwater head.

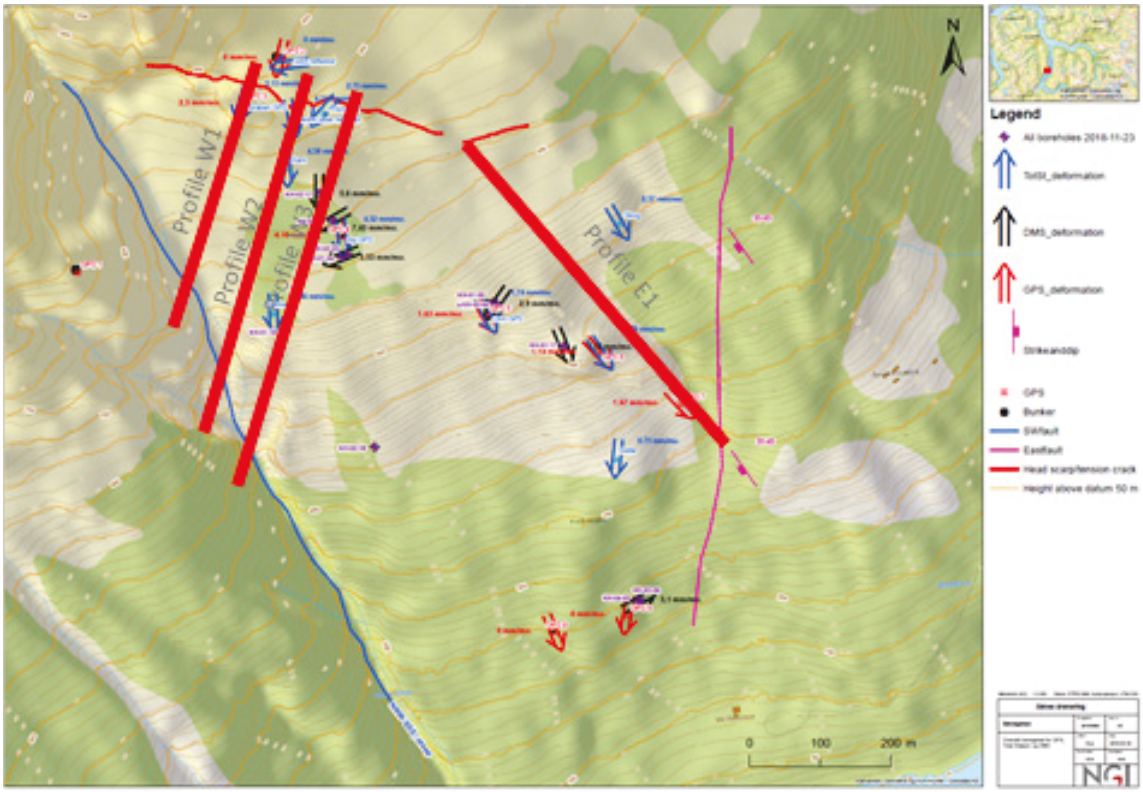

Figure 2 Location of cross-sections. W2 and E1 were used in the numerical modelling.

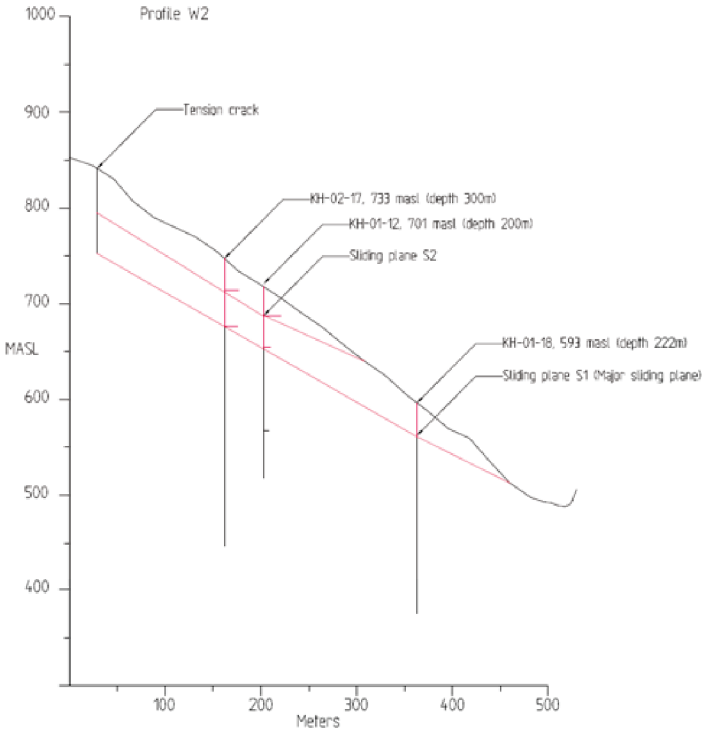

Figure 3 Cross-section W2.

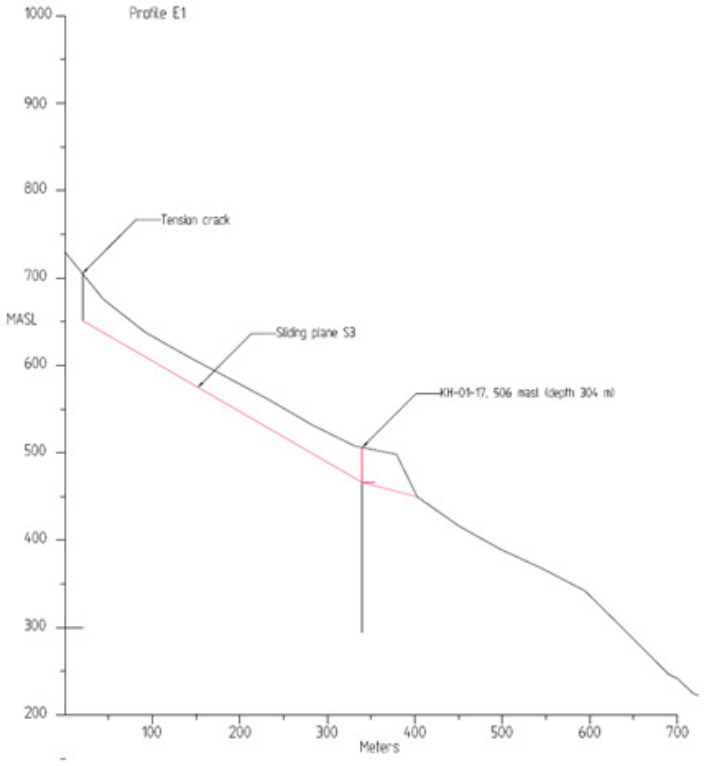

Figure 4 Cross-section E1.

3.1 Rock mass properties

The Åknes rock slope consist of biotitic gneiss, granitic gneiss and dioritic gneiss. Several tests on intact rock have been carried out, including uniaxial and triaxial tests. An example of results is shown in Figure 5. As it is visible, the strength of the intact rock varies significantly, dependent on rock type. Therefore, to have a better understanding, it is required to focus on the intact rock mass which are adjacent to the sliding planes. Analyses of the core pictures show that the rock mass close to the sliding planes are mafic and dark coloured with small grain size. Mineralogically the rock is similar to the rest of the rocks in the study site and can be classified as dioritic gneiss [12]. The results of the axial and triaxial compression tests of the intact rock adjacent the sliding planes is shown in Figure 6 and the results are also presented in Table 1.

The intact rock adjacent the sliding planes is weaker than other rock types tested in the study site; compare Figure 5 and Figure 6. The intact rock tests reported in Figure 5 are from samples which were selected along the available boreholes without focusing on the intact rock adjacent the sliding planes.

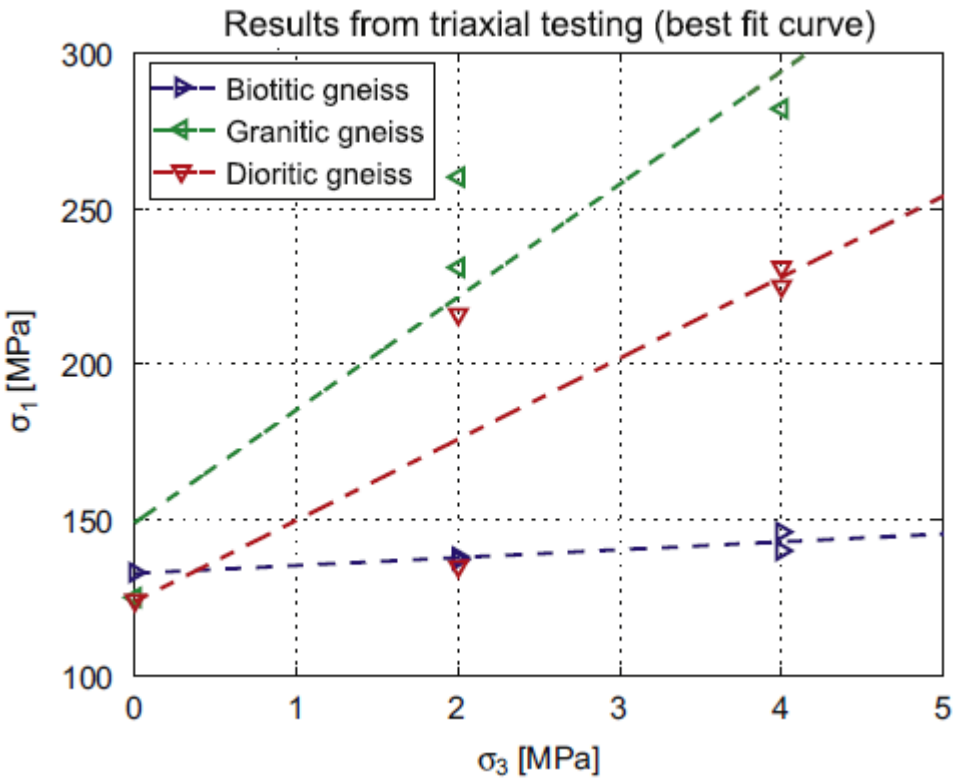

Figure 5 Results of the uniaxial and triaxial tests carried out on different rock samples from Åknes [11].

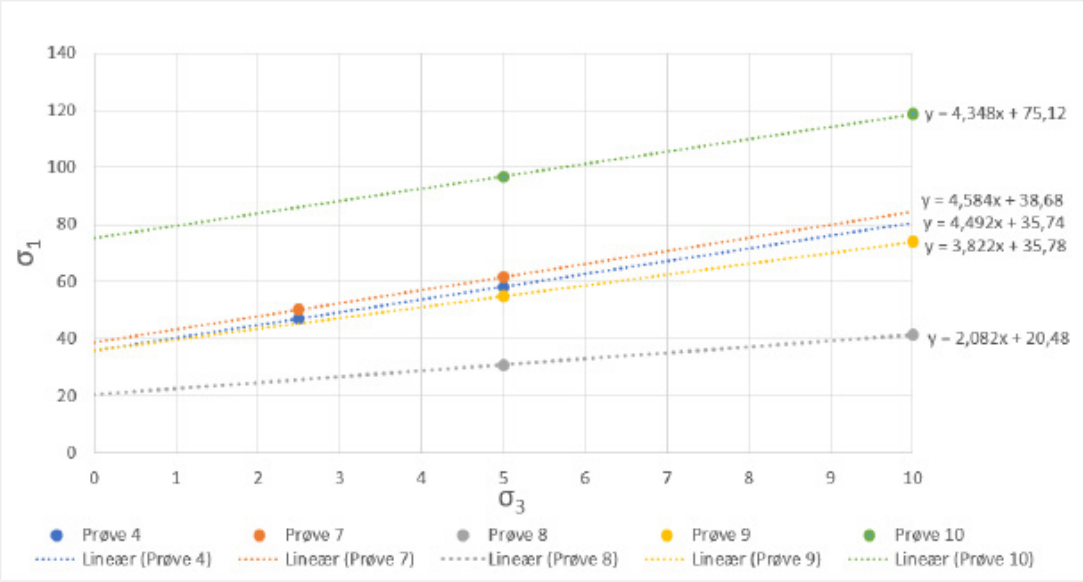

Figure 6 Results of triaxial tests on intact rock adjacent the sliding plane [12].

Since the slope movement and water transport at Åknes is controlled by the discontinuities, the rock blocks are obeying elastic behaviour in the numerical modelling. Therefore, Young's modulus and Poisson's ratio of the intact rock are used in the numerical models. It was reported by previous laboratory tests on the intact rocks of the study site that the intact rock has mean Young's modulus between 38.7 to 40 GPa [6, 13] which is correlating with the recently measured values for the intact rock adjacent the sliding planes [12]. Therefore, the mean value of elastic properties reported in Table 1 were used in the numerical modelling.

Table 1 Mechanical properties of the intact rock adjacent the sliding planes.

Property	Mean value	Standard deviation	Ref.
Uniaxial compressive strength (MPa)	69.50	24.9	[12]
Intact rock Young's modulus (GPa)	40.0	6.5	[12]
Inherent cohesion of intact rock (MPa)	11.10	4.0	[12]
Inherent friction angle of intact rock (Degrees)	38.5	1.60	[12]
Poisson's ratio (-)	0.2	-	[11 and 13]

According to ISRM (1978) [21] following data from each discontinuity should be mapped and recorded:

1. Orientation: Attitude of discontinuities in space. Described by dip / dip-direction.
2. Spacing: Perpendicular distance between adjacent discontinuities. Normally refers to the mean or modal spacing of a set of joints
3. Persistence: Inherent trace length as observed in an exposure. May give a crude measure of the real extent or penetration length of a discontinuity. Termination in solid rock or against other discounted reduces the persistence.
4. Roughness: Inherent surface roughness and waviness relative to the mean plane of a discontinuity.
5. Wall strength: Equivalent compression strength of the adjacent rock walls of a discontinuity.
6. Aperture: Perpendicular distance between adjacent rock walls of a discontinuity, in intervening space is air or water filled.
7. Filling: Materials that separates the adjacent rock walls of a discontinuity.
8. Seepage: Water flow and free moisture visible in individual discontinuity or in the rock mass as whole.
9. Number of sets: The number of joint sets comprising the intersecting joint system.
10. Block size: Rock block dimensions resulting from the mutual orientation of intersecting joint sets and resulting from spacing of the individual sets.

Here we review those parameters reported by different authors and suggest appropriate values that will be used for the numerical modelling.

In general, it is reported that at Åknes there is three joint sets: foliation parallel discontinuities and two vertical joints sets with strike in NS and EW directions [6, 9, 10 and 15].

In most of the reported studies from Åknes rock slide "fracture frequency" was reported rather than spacing of each discontinuity set [6, 9, 10 and 15]. "Fracture frequency" is referred to as total number of discontinuities in one meter at a specific direction (for example a vertical borehole or a scan line) which makes it challenging to transform it into spacing of each individual discontinuity set. It should be noted that for the numerical modelling we need mean spacing of each discontinuity set.

Based on scanline mapping at the study site Kveldsvik et al. (2007) [14] reported that the average number of foliation parallel joints are 2 fractures / meter for fractures with persistence larger than 1 m. However, they concluded that the fracture frequency in direction perpendicular to the strike of the foliations is around 2.4 fracture / m. They also reported that several foliation parallel joints were encountered with length of several decimetres but did not consider those in the calculating of the fracture frequency. They also reported that fracture frequency for the vertical fractures is about 1 fracture / m.

Ganerød et al. (2008,) [15] reported that the fracture frequency from scanlines is about 2 – 8 and 8 – 12 fractures / m in directions of parallel and perpendicular to the major foliations, respectively. In addition, they reported that from the boreholes, the fracture frequency varies from 1 fracture / m to 50 fracture / m. They also reported that the most common fracture frequency is 8 – 12 fracture / m. For us, it is not clear what is meant technically with the terminology " the most common fracture frequency". However, it was interpreted as the mean fracture frequency. In the evaluations of the fracture frequency reported in this article, the crushed zones were assumed as zones with high fracture frequency which led to fracture frequency of 50 fracture per meter.

Grøneng et al. (2010) [11] reported based on cores from 10 available boreholes that the fracture frequency is high in first 70 m of the boreholes reaching fracture frequency of 10 fracture / m.

Ringstad (2019) [16] carried out extensive studies of discontinuity network in Åknes by mapping on the ground surface. He noticed that in the west flank and east flank of Åknes the average frequency for foliation parallel discontinuities (joint set 1), and vertical joint with strike in NS (joint set 2) and vertical joint set with strike in EW directions (joint set 3) are 7.1, 4.5 and 3 [joints/m], respectively. His data shows that just 49% of the mapped joints have ends which are connected to other joints. It means that almost 50% of the mapped joints are involved in joint network which is important for stability of the slope and water transportation and the rest are isolated fractures.

In summary following values of fracture frequency were reported:

- Mean value of 8- 12 fracture /m at which it can reach 50 fracture / m from boreholes and 23 fracture / m from scanlines (Ganerød et al. (2008) [15])
- Fracture frequency of 10 fracture / m from boreholes in first 70 m of the boreholes (Grøneng et al. (2010) [11])
- 2.4 fracture / m perpendicular to the strike of the foliations (Kveldsvik et al. (2007) [14])
- Joint sets 1, 2 and 3 has joint frequency of 7.1, 4.5 and 3 joint / m while just 50% of them interconnected to the joint sets and rest of them are isolated joints. It means that the effective joint frequency should be used in the analysis is 3.5, 2.2 and 1.5 joint /m for joint sets of 1, 2 and 3, respectively. The corresponding mean joint spacing for joint sets 1, 2 and 3 are assumed 0.28, 0.45 and 0.67 m, respectively. It should be noted that the field measurements reported by Ringstad shows lognormal distribution which has large variations. Therefore, this estimation of the joint frequency is conservative for the rock mass at Åknes.

As presented above there are considerable differences between the reported values which makes it very challenging to understand and use them in the numerical models. In addition, most of the reported values are for fracture frequency and the required value in the numerical modelling is mean joint spacing (or mean joint frequency) for each individual joint set. Moreover, several of the references considered the crushed zones (weakness zones) into the fracture frequency as a zone with high fracture frequency. This assumption can lead to overestimation of the fracture frequency. Between all the available references, studies by Ringstad (2019) is more detailed and covers what is needed for the numerical modelling. Therefore, the values reported by Ringstad (2019) were used in the numerical modelling.

The block volume can be estimated by:

$$V = \prod_{i=1}^{n} S_i \qquad \text{(Eq. 1)}$$

Where
n: total number of joint sets at the study site = 3
i: number of joint set
Si: mean spacing of joint set i.

Mean block length of rock mass can be estimated by:

$$l = \sqrt[3]{V} \qquad \text{(Eq. 2)}$$

Using the given data above and Eq. 1 and 2, the mean block length at the ground surface is about 0.44 m. This value is close to the smallest block length reported by Ringstad (2019) and almost half of the mean block length (0.83 m), see Table 2. This difference comes from the fact that the distribution of the joint spacing in each mapping station is not normal and it has very large deviation. Therefore, we used block length calculated in Table 2 as the reference to joint spacing in the numerical models. As a result, it was

decided in the numerical modelling that the mean joint spacing for joint sets 1, 2 and 3 is 0.56, 0.90 and 1.34 m, respectively, which is two times of the reported mean joint spacing by Ringstad (2019). Moreover, using all those upper mentioned joint spacings in the UDEC models makes the run time of the models unrealistically high. Therefore, we modelled the joint spacing with the upper mentioned values just close by the sliding plane.

Ganerød et al. (2008) [15] reported joint length of joint sets of 1, 2 and 3 as 5-10, 2-5 and 1-2 m, respectively. We assume that joint length is the joint persistence. There is no other reporting regarding joint persistence. Therefore, in the numerical modelling it was assumed that the mean persistence of joint sets 1, 2 and 3 are 10, 5 and 2 m, respectively.

Table 2 Minimum, mean and maximum block volume reported by Ringstad (2019) at 40 locations at Åknes.

Location	Min. block volume (m^3)	Mean block volume (m^3)	Max. block volume (m^3)
1	0.1	1	4
2	0.05	1.5	5.25
3	0.01	0.7	1.45
4	0.2	1	5.5
5	0.05	0.4	1
6	0.2	0.5	2.9
7	0.01	1	10
8	0.0025	0.1	1
9	0.0015	0.05	0.5
10	0.15	1	2
11	0.1	2	3
12	0.01	0.3	1
13	0.005	0.3	3.7
14	0.03	0.5	1.2
15	0.05	0.5	4
16	0.01	0.5	1
17	0.002	0.4	0.9
18	0.005	0.4	3
19	0.001	0.4	0.6
20	0.1	0.7	3.75
21	0.1	0.5	3
22	0.2	0.5	4
23	0.1	0.3	2.5
24	0.05	0.2	1
25	0.02	0.2	0.5
26	0.0025	0.5	1
27	0.003	1	2

Location	Min. block volume (m^3)	Mean block volume (m^3)	Max. block volume (m^3)
29	0.2	0.5	1
30	0.001	0.02	0.15
31	0.024	0.36	2.9
32	0.015	1.5	7.5
33	0.0038	0.25	5.4
34	0.0072	1.44	9.7
35	0.006	0.55	2.9
36	0.009	0.15	3.9
37	0.002	0.3	1.44
38	0.0012	0.46	3
39	0.0025	0.018	0.8
40	0.03	0.3	0.8
Mean block volume (m^3) *	0.047	0.57	2.80
Block length (m) **	0.36	0.83	1.41

* Mean value of each column **Used Eq. 2

Roughness of joints measured in small scale (10 cm length profiling) and large scales (several meters length) are denoted as JRC_0 and JRC_n, respectively. For the numerical modelling we need value of JRC_n which is normalised by the scale effect of joint length (Table 3).

Similarly, JCS value which is estimated by Schmidt hammer is called JCS_0 which later normalised via Barton et al. (1985) [4] technique to the joint length and denoted as JCS_n. In this report we are using JCS_n, which is reported in Table 3.

Unfortunately, there is no report regarding joint physical aperture (hereafter denoted as physical aperture to differentiate from hydraulic aperture); and the available reports are mostly covering the hydraulic aperture of the rock joints. Based on field hydraulic tests by Frei (2008) [17], the hydraulic aperture of the joint system is 140 µm. This value is based on back calculation of water flow from springs in the west side of the rock slope. Barton et al. (1985) [4] suggested the following relation between hydraulic and mechanical aperture of rock joints:

$$a_0 = \frac{JRC^{2.5}}{(\frac{a_j}{a_0})^2} \qquad \text{(Eq. 3)}$$

Where
a_j is joint physical aperture in µm
a_0: joint hydraulic aperture in µm

Using Eq. 3 and JRC_n=8.2 leads to physical aperture of 164 μm. This estimation is used in the numerical modelling. But it should be noted that the best way to estimate the physical aperture is from field mapping (special rulers can be used), not the technique described here. Nevertheless, due to lacking data, we used it.

In addition to the parameters mentioned by ISRM (1978) to map rock joints, normal stiffness and shear stiffness of the joints are also required in the numerical model. The normal stiffness and shear stiffness of the discontinuities was calculated based on Barton-Bandis model [4]. Joint normal stiffness is connected to the normal stress: with increased normal stress the normal stiffness also increases. However, when the normal stress level is low, joint closure versus normal stress is linear, which can be used to define an initial normal stiffness for joints:

$$K_{ni} = -7.15 + 1.75\,JRC + 0.02\left(\frac{JCS}{a_j}\right) \quad \text{(Eq. 4)}$$

Where:
K_{ni}: Initial joint stiffness of joints (GPa /m)
JRC: Joint roughness coefficient
JCS: Joint wall compression strength (MPa), and
a_j: joint mechanical apertures (mm).

Shear stiffness of joints is also dependent on the stress level and roughness of the joint surface. Barton et al. (1985) [4] found by intensive laboratory testing that when the normal stress is larger than ca. 0.25 MPa, the shear stiffness is approximately 1/10 of the normal stiffness. Therefore, a good initial approximation can be obtained by the following formula:

$$K_s \approx \frac{1}{10}\,K_n \quad \text{(Eq. 5)}$$

Where Ks is in GPa/m.

According to Barton and Choubey (1977) [18] shear resistance of the joints can be estimated by:

$$\tau = \acute{\sigma_n} \tan\left(\varphi_r + JRC\ log\left(\frac{JCS}{\acute{\sigma_n}}\right)\right) \quad \text{(Eq. 6)}$$

Where:
$\acute{\sigma_n}$: Effective normal stress,
φ_r : Residual friction angle
JRC: Joint roughness coefficient
JCS: Joint wall compression strength.

Since the normal stress on the joint network above the sliding planes and on the sliding planes is smaller than 1 MPa, it is possible to calculate a representative friction angle for the rock joints, as demonstrated in Figure 7. Using Eq. 6 the shear resistance was

calculated for normal stresses smaller than 1 MPa. Later, a best fitting line that passes from the origin of the stress coordinate system was fitted on the data. The tangential angle of the linear formula is the tangent of the friction angle for joint. Therefore, the rock joints in the numerical models were assumed to have friction angle of 39.6 degrees while their cohesion and tensile strength is zero.

As shown in [2] the majority of the DMS data shows that sliding happens in a localised section inside the rock mass, denoted as sliding planes. Therefore, the sliding planes have shearing resistance which is less than the rock joints. This leads to the fact that back-calculated friction angle of the sliding plane from the numerical models should be less than 39.6 degrees.

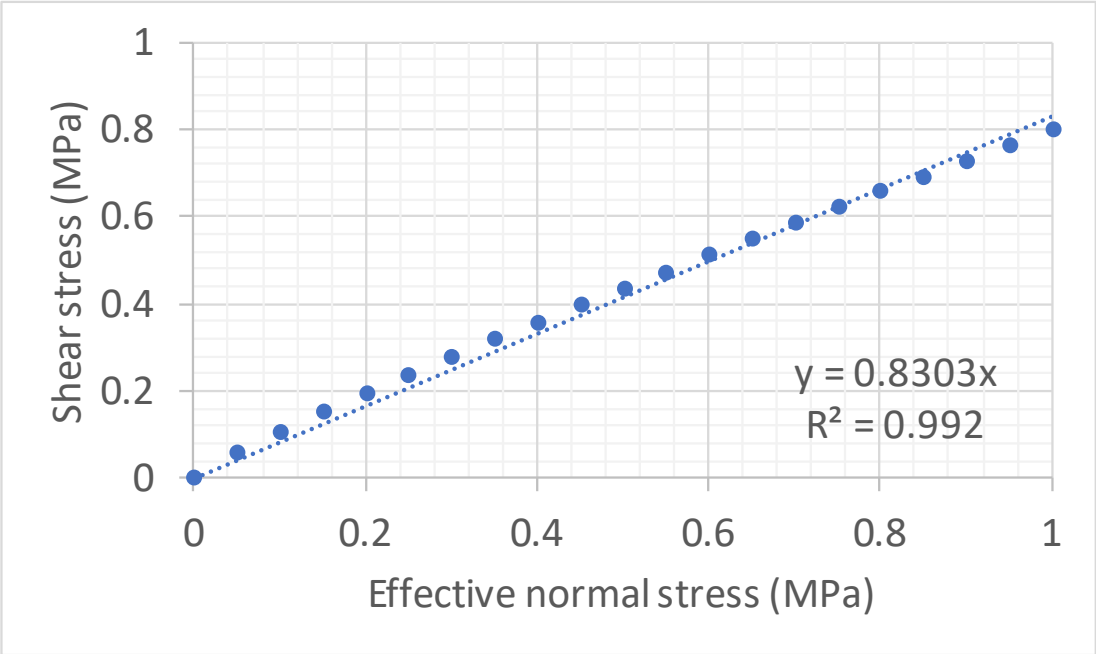

Figure 7 Calculating a representative friction angle for rock joints.

The discontinuities in Åknes rock slide are the water transporting channels. The water flow in the discontinuities is governed by the cubic law [4] which assumes that the joints are parallel planes. According to Barton et al. (1985) [4], the hydraulic aperture is associated also with effective normal stress (see a simplified format in Figure 8). When increasing the normal stress, the hydraulic aperture decreases and reaches a smaller value which is called residual hydraulic aperture (a_{res}).

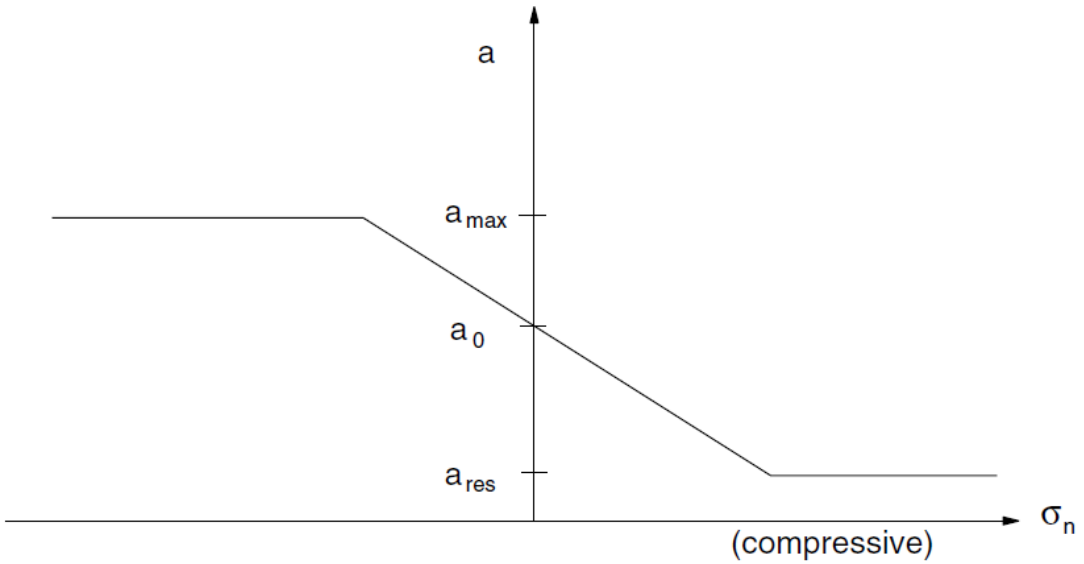

Figure 8 Changes in the hydraulic aperture (a) of the rock joints with normal stress [19].

Based on the field investigations carried out by Frei (2008) [17] the hydraulic opening of the water transporting channels in Åknes at the west flank is 0.14 mm (140 µm) which was used as initial hydraulic aperture (a_0) in the numerical modelling. It can be argued that the back-calculation of (a_0) was done based on water flow from springs occurring where the overburden is low, and the area is likely to have low stress level due to the shallow depth. Since there is no laboratory testing on rock joints to assess the residual hydraulic aperture, a rule of thumb was used. It was suggested by ITASCA (2014) [19] the residual hydraulic aperture (a_{res}) of the rock joints can be assumed to be 1/5 of the initial hydraulic apertures (a_0), and this is used in the numerical modelling.

In the numerical modelling another parameter is required which is called joint gap; it represents the spacing of joints in parallel direction to their strike. Since this parameter has not been mapped in the reported studies, it was assumed that joint gap is equal to the joint spacing in the numerical model. Table 3 presents a summary of rock joint properties at Åknes.

Table 3 Properties of the joint sets in Åknes.

Properties	Joint set 1	Joint set 2	Joint set 3	Comment
Type	Foliation parallel	Joint	Joint	
Dip / Dip-Direction	31 / 153	90 / 267	90 / 011	
Mean Spacing (m)	0.56	0.9	1.34	
Joint Gap (m)	0.56	0.9	1.34	
JRC_n	8.2 (2.6)	8.2 (2.6)	8.2 (2.6)	
JCS_n (MPa)	60 (17)	60 (17)	60 (17)	
Basic friction angle (°)	30.9	30.9	30.9	Based on tests from [12]
Residual friction angle	24	24	24	Based [6 and 9]
Normal stiffness (GPa/m)	14.7	14.7	14.7	Eq. 4
Shear stiffness (GPa/m)	1.50	1.50	1.50	Eq. 5
Physical aperture - a_j (mm)	0.16	0.16	0.16	
Hydraulic apertures - *a0* (mm)	0.14	0.14	0.14	
Residual hydraulic apertures - a_{res} (mm)	0.03	0.03	0.03	

* Values inside parenthesis represents the standard deviation of the values.

3.2 Hydraulic setting

In hard rocks like gneiss the porosity of the intact rock mass is very low as also demonstrated in Tønset (2019). Tønset (2019) showed that rock samples from Åknes have same density in saturated and dry conditions meaning that the effective porosity of the intact rock is neglectable. Therefore, the water transportation system is the interconnected discontinuity network. Based on the hydrogeology report [1], the rock mass has well developed hydraulic communications system. The measured ground water table in the boreholes are as presented in Table 4. Among the available boreholes, borehole KH-01-2012, KH-02-2017 and KH-01-2018 show groundwater table which is standing on the sliding plane at the west flank. Borehole KH-01-2017 shows between zero to 0.5 m water head standing on the sliding plane at the east flank.

Table 4 Groundwater head on the sliding plane measured in different boreholes [2].

Borehole number	No. of piezo-meters	Water table* (mbgl)	Depth to main sliding plane (mbgl)	Water pressure on main sliding plane (m)
KH-01-06	1	55-60	49-50	0
KH-02-06	1	43,7-45,7	33	0
KH-03-06	1	41,5-44	24	0
KH-01-12	1	~62	62	0-2,7
KH-01-17	9	~35,3	35,5	0-0,5
KH-02-17	11	~66,5	70	2,3-3,5
KH-01-18	10	~33,4	34	0,4-1,4
KH-02-18	12	~18	15	0

*Meters below ground level.

4 Numerical modelling

4.1 Model setup

To include effect of the groundwater on the stability analysis a coupled hydro-mechanical approach (HM) is used. In the modelling, groundwater is transported only through the interconnected discontinuity network.

The model has two major discontinuity systems: the sliding plane and three joint sets (Table 3). The sliding plane was modelled as a large persistent discontinuity having just frictional resistance, since it is fully developed in large sections of the rock slope (as presented in [2]).

Summary of mechanical properties for intact rock and discontinuities used in the numerical modelling are presented in Table 5.

Table 5 Summary of the input data implemented in the numerical models.

Parameter	Unite	Value
Young's modulus of intact rock	GPa	40
Poisson's ratio of the intact rocks	-	0.2
Rock density	MN/m^3	0.027
Friction angle of the joint system	Degree	39.6
Cohesion of the joint system	MPa	0
Tensile resistance the joint system	MPa	0
Normal stiffness of discontinuity	GPa/m	14.7
Shear stiffness of discontinuity	GPa/m	1.50
Initial hydraulic aperture (a_0)	(mm)	0.14
Residual hydraulic aperture (a_{res})	(mm)	0.03

The following steps were used to build the numerical model:

1. Geometry of the model was built up including rock joint network and sliding surface.
2. Let the model run and generate in-situ stress state inside the rock mass assuming only gravity and elastic response of rock. The mechanical boundary conditions are roller boundaries in left- and right-hand side boundaries and totally fixed boundary in the bottom of the model. The model's upper boundary (the slope surface) is free.
3. Generating the groundwater head inside the rock mass using the data from available boreholes on each cross-section (Table 4 in Chapter 3.2).
4. Back-calculating the frictional resistance of the sliding plane.

The rock joint spacing in the models follows the values mentioned in Table 3 just in the area close by the sliding plane. For rest of the regions, the joint spacing gradually increases from 5 to 8 times of those values dependent on their distance from the sliding surface.

4.2 Hydro-mechanical numerical modelling and boundary conditions

The hydraulic boundary condition of the models is shown in Figure 9. Left and right boundaries are assigned with the hydrostatic water head. The lower boundary is impermeable while upper boundary is free. No water infiltration into rock mass from the ground surface was considered in the modelling. The water height at the left- and right-hand side in the model is selected in a way which lead to same water tables as measured in the available boreholes in the cross-section. The presented boundary condition (Figure 9) is selected because:

- There is hydraulic communication between rock masses located above and below the sliding planes (for further details check [1 and 17]. In addition, hydraulic communications can be extended to the rock mass located in the northern part of the backscarp since there is no geological feature which can isolate the rock mass in the unstable part from the rest of the mountainside.
- There exist several springs north of the backscarp in the higher elevations showing flowing groundwater also north of the backscarp (Figure 19).

After assigning the hydraulic boundary conditions (implying the water head in the left and right hand-side boundaries of the model), the model runs until the water flow inside the model reaches steady state condition; meaning that the water flow rate does not change with time. After reaching steady state condition, the water table in the locations of the available boreholes were checked. If the water head from the model coincides with measurements in the boreholes then the assumed hydraulic boundary condition is valid, and then modelling continues to back-calculate the frictional resistance of the sliding plane.

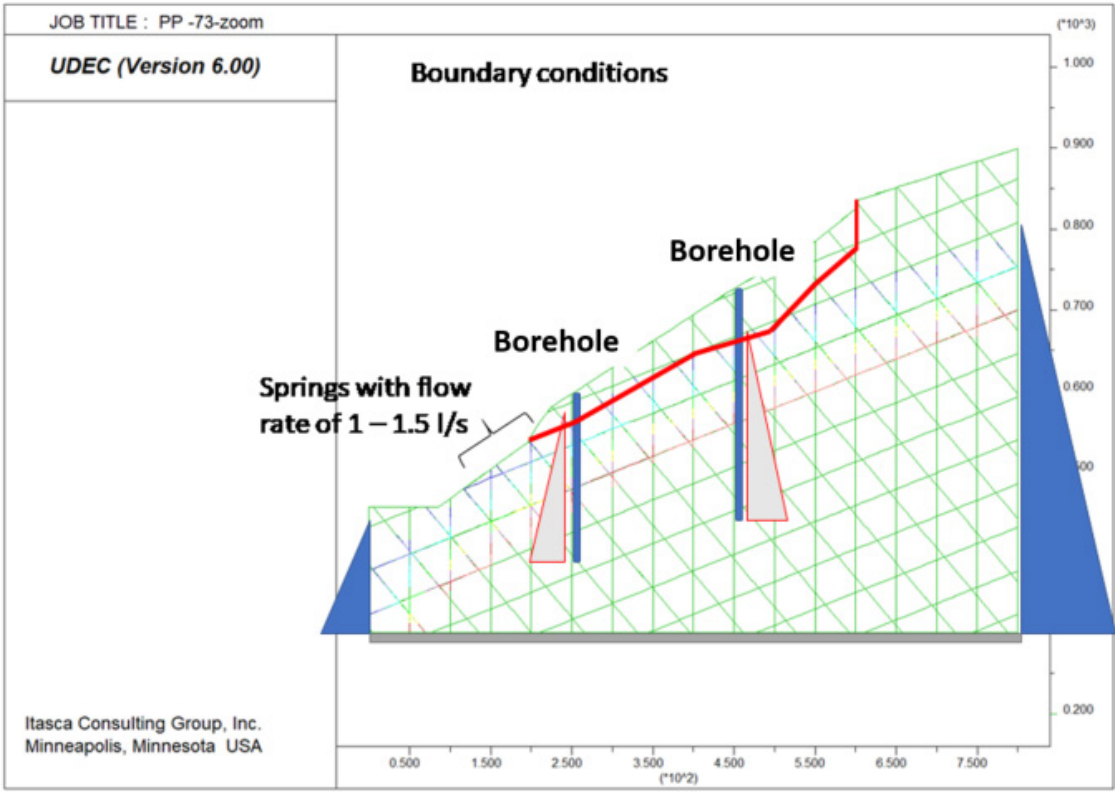

Figure 9 Hydraulic boundary conditions in the models.

4.3 Back-calculation of current condition in cross-section W2

4.3.1 Modelling the groundwater condition in cross-section W2

The geometry of the model is shown in Figure 10. A zone around the sliding plane was modelled with the exact joint network geometry suggested in Chapter 3. The modelling steps were followed as written in Chapter 4.1.

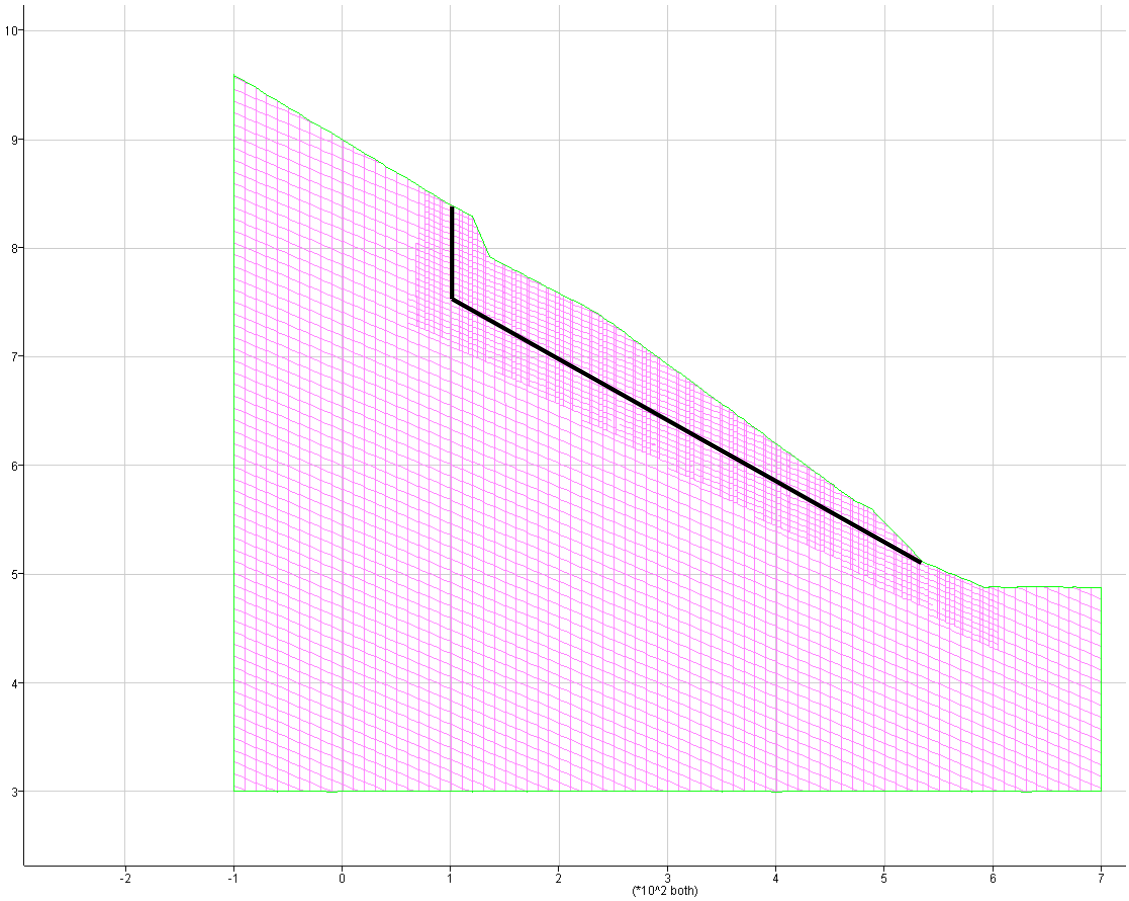

Figure 10 Geometry of the UDEC model for cross-section W2. Black lines are representing the backscarp and sliding surface.

Figure 11 shows the cross-section with the used hydraulic boundary conditions and calculated water head acting on the sliding plane. The numerical model shows that the highest water head on the sliding plane is located at the back scarp (17 m). The water head decrease with descending surface elevation. It reaches zero at the sliding surface on elevation approximately 630 m.a.s.l. Downwards, the water table mostly follows the sliding plane (ca. zero water head on the sliding surface) continuing toward the toe of the sliding plane.

The adapted boundary conditions in Figure 11 generates 3.5 m, 2 m and 0 m water head on the sliding plane at the location of boreholes KH-02-2017, KH-01-2012 and KH-01-2018, respectively.

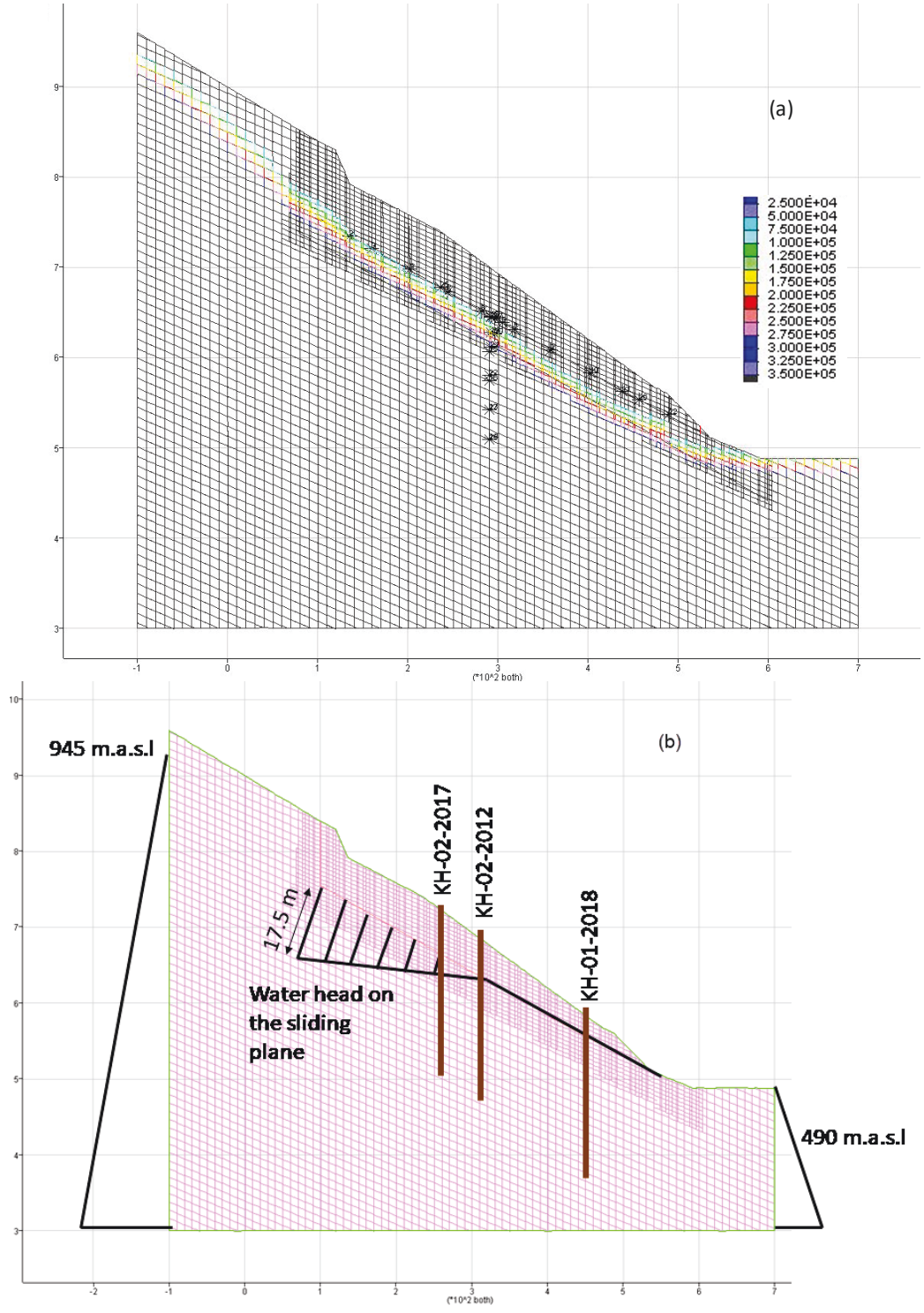

Figure 11 (a) Hydraulic results from numerical modelling: green contour shows where groundwater head is ca. 10 m. For visualisation purpose the maximum pore pressure is limited to 3.5E5 Pa (35 m of water head); (b) illustrating the assumed hydraulic boundary conditions and resulted water head distribution over the sliding plane.

4.3.2 Back calculating frictional resistance of sliding plane in cross-section W2

The purpose of the modelling was to back calculate the frictional resistance of the sliding surface, as today's condition. Therefore, after generating the groundwater pressure inside the model (as illustrated in Figure 11), the factor of safety (FOS) of the model was calculated for some assumed trial values (Table 6). With calculated factor of safety for each trial friction angle, it is possible to calculate the frictional angle which leads to FOS = 1:

$$\tan(\varphi) = \frac{1}{FOS} \tan(\varphi^{trial}) \qquad (7)$$

Table 6 presents different assumed trial friction angles and calculated friction angle for the sliding surface resulting in FOS = 1. As it is demonstrated with two different trials, with today's condition, the sliding surface has friction angle of 31.93 degrees for factor of safety equal 1.00.

Moreover, using the back calculated friction angle of 31.93 degrees for the sliding surface and totally draining the water out of the rock slope, increases the factor of safety from 1.00 to 1.04.

Table 6 Results of coupled hydro-mechanical stability analysis of cross-section W2.

Try number	Assumed friction angle (degrees)	Assumed cohesion (kPa)	Ground water condition	Calculated factor of safety from UDEC	Corresponding friction angle for FOS = 1.00
1	31	0	As in Figure 11	0.96	31.93
2	28	0	As in Figure 11	0.83	31.93
3	31.93	0	Totally dry	1.04	-

4.4 Back-calculating of current condition in E1

4.4.1 Modelling the groundwater condition in cross-section E1

The geometry of the model is shown in Figure 12. The joint network was modelled as demonstrated in Chapter 3. The modelling steps as written in Chapter 4.1 were followed.

Figure 13 shows the cross-section with the used hydraulic boundary condition and calculated water head acting on the sliding plane. The numerical model shows that the highest water head on the sliding plane is located at the middle of the sliding plane (5 m).

The waterhead follows changes in the topography of the cross-section and it leads to have 1 m of water head on the sliding plane at the location of KH-01-2017.

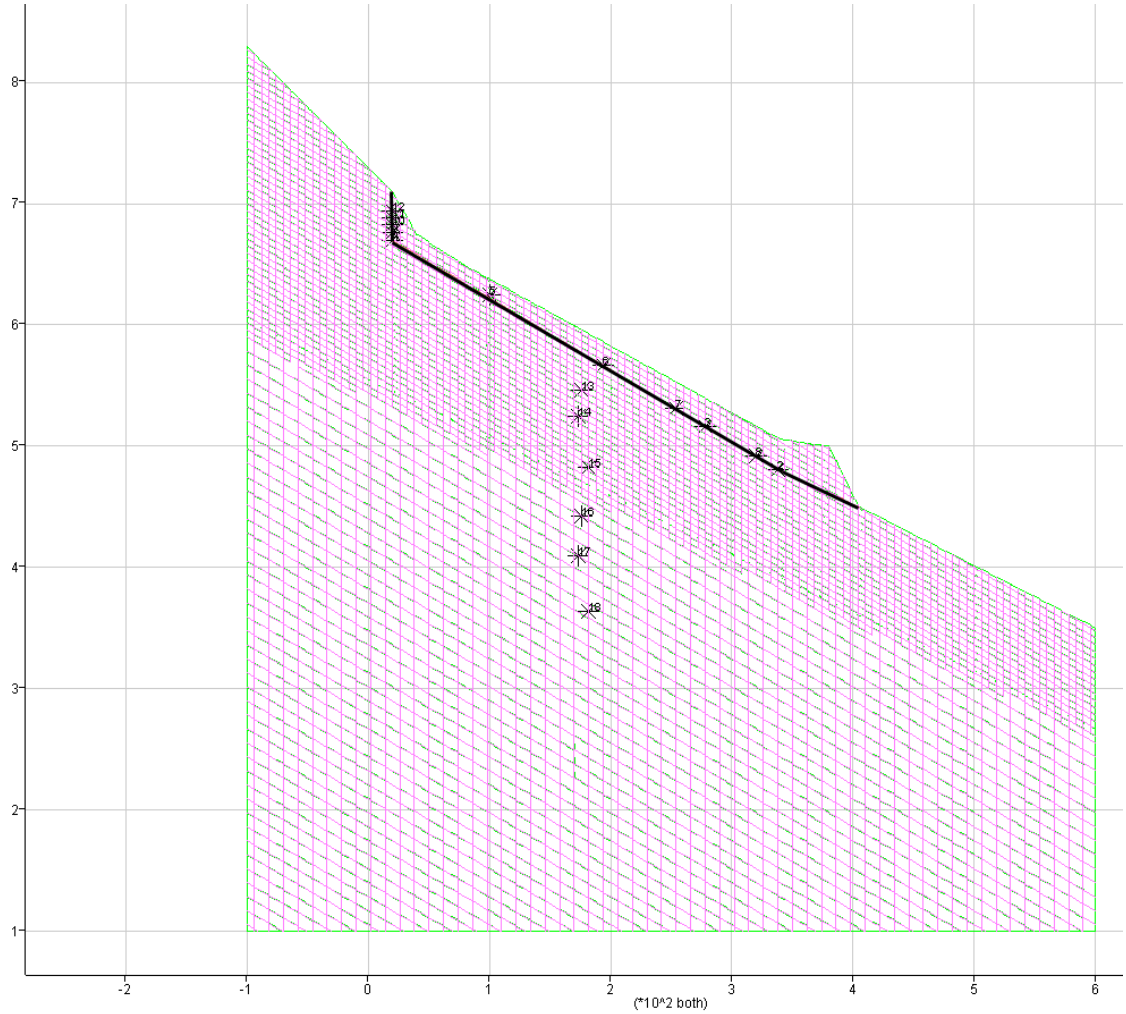

Figure 12 Geometry of the UDEC model for cross-section E1. Black lines are representing the backscarp and sliding surface.

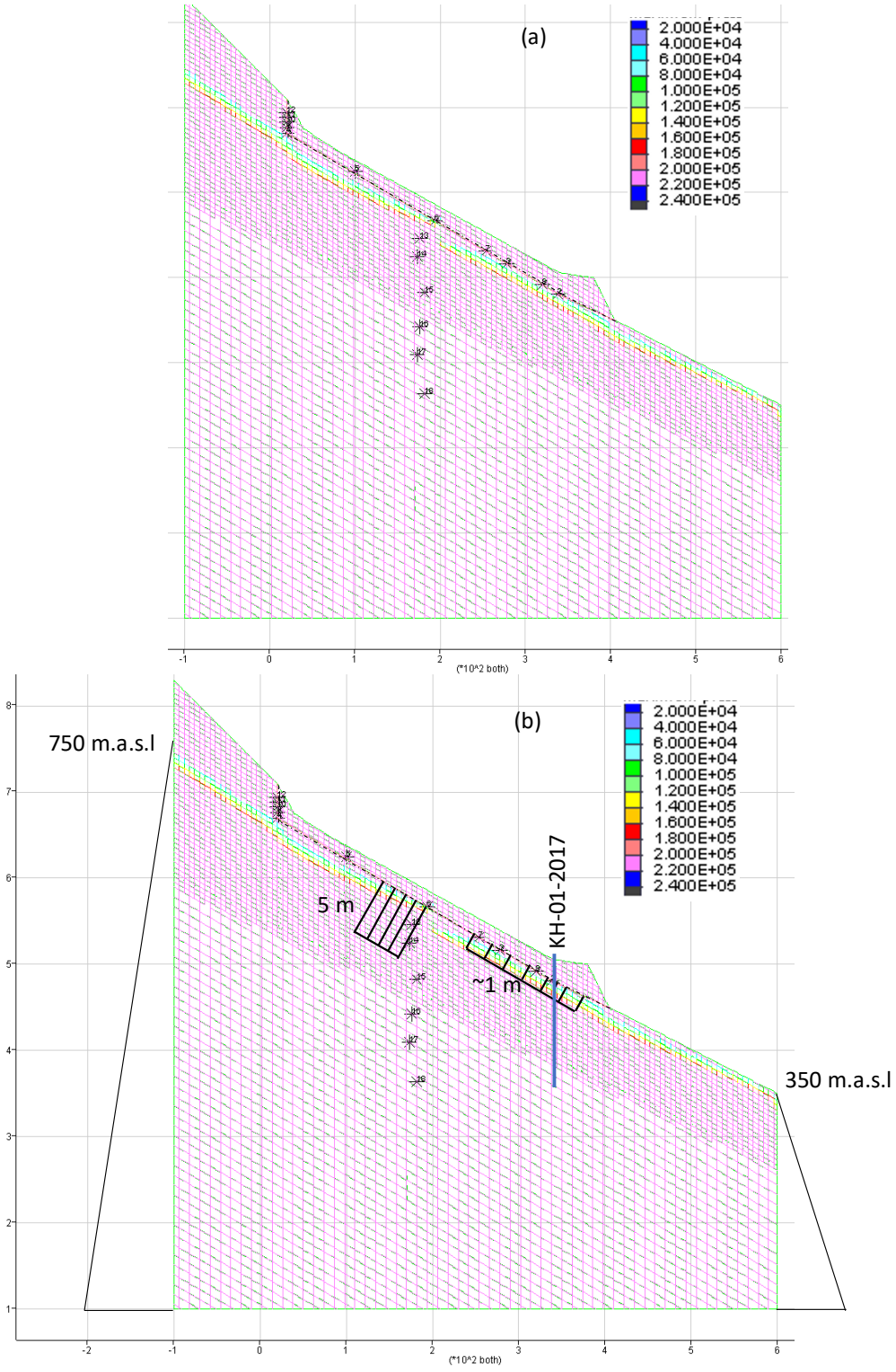

Figure 13 (a) Hydraulic results from numerical modelling: green contours shows where groundwater head is ca. 6 m. For visualisation purpose the maximum pore pressure is limited to 2.4E5 Pa (24 m of water head); (b) illustrating the assumed hydraulic boundary conditions and resulted water head distribution on the sliding plane.

4.4.2 Back calculating frictional resistance of sliding plane in cross-section E1

Results from factor of safety calculations in UDEC for the cross-section E1 is presented in Table 7. Assuming a factor of safety = 1.00 the sliding plane has frictional angle of 27 degrees.

Fully draining the model will increase the factor of safety by 0.5%.

Table 7 Results of coupled hydra-mechanical stability analysis of cross-section E1.

Try number	Assumed friction angle (degrees)	Assumed cohesion (kPa)	Ground water condition	Calculated factor of safety from UDEC	Corresponding friction angle for FOS = 1.00
1	32	0	As in Figure 14	1.22	27
2	27	0	Totally dry	1.005	-

5 Discussions

Back-calculations of the groundwater status and the frictional resistance of the sliding surface were carried out in chapter 4. In this chapter, the numerical results will be discussed.

First, the correlation between two modelled cross-sections W2 and E1 in terms of hydraulic head will be discussed. They will also be compared with field observations.

Second, an assessment on how fast rising of the water in the backscarp, can affect the stability of the slope will be presented. This is carried out only for cross-section W2 where the backscarp is open and deep.

Finally, a hypothetical situation will be presented where the groundwater head raised to its highest theoretical level and then, the stability of Åknes rock slope in such situation was investigated.

5.1 Correlating water head in the west and east flanks

As numerical modelling showed (Figure 11 and Figure 13), the groundwater flows through the foliation parallel joints; i.e. the main water transporting channels is the foliation parallel joint set.

Assume that foliation parallel joints passing from the backscarp in cross-section W2 has long enough persistence to reach the backscarp in cross-section E1. As illustrated in Figure 14, the dashed lines presenting the strike of a joint belonging to the foliation parallel joint set pathing from backscarp in the cross-section W2. If the joint has dip angle of 31 degrees and horizontal distance between the two marked strike lines is 150

m, there should be ca. 90 m descending in the elevation of the joint from cross-section W2 to E1. As a result, the groundwater head in the joint should descend ca. 90 m by flowing from the location of the cross-section W2 to E1 (considering that the water velocity is neglectable). Hence, the water table numerically calculated at the backscarp of E1 should have ca. 90 m lower elevation compared to W2.

Numerical modelling shows that the groundwater table in the backscarp of the cross-section W2 is located at elevation of 780 m.a.s.l. Therefore, the water table in the backscarp of the cross-section E1 should be at elevation 780 – 90 = 690 m.a.s.l. which is coinciding with Figure 13. Hence, the numerical models with the chosen boundary condition have captured the hydraulic connection of the slope around the backscarp.

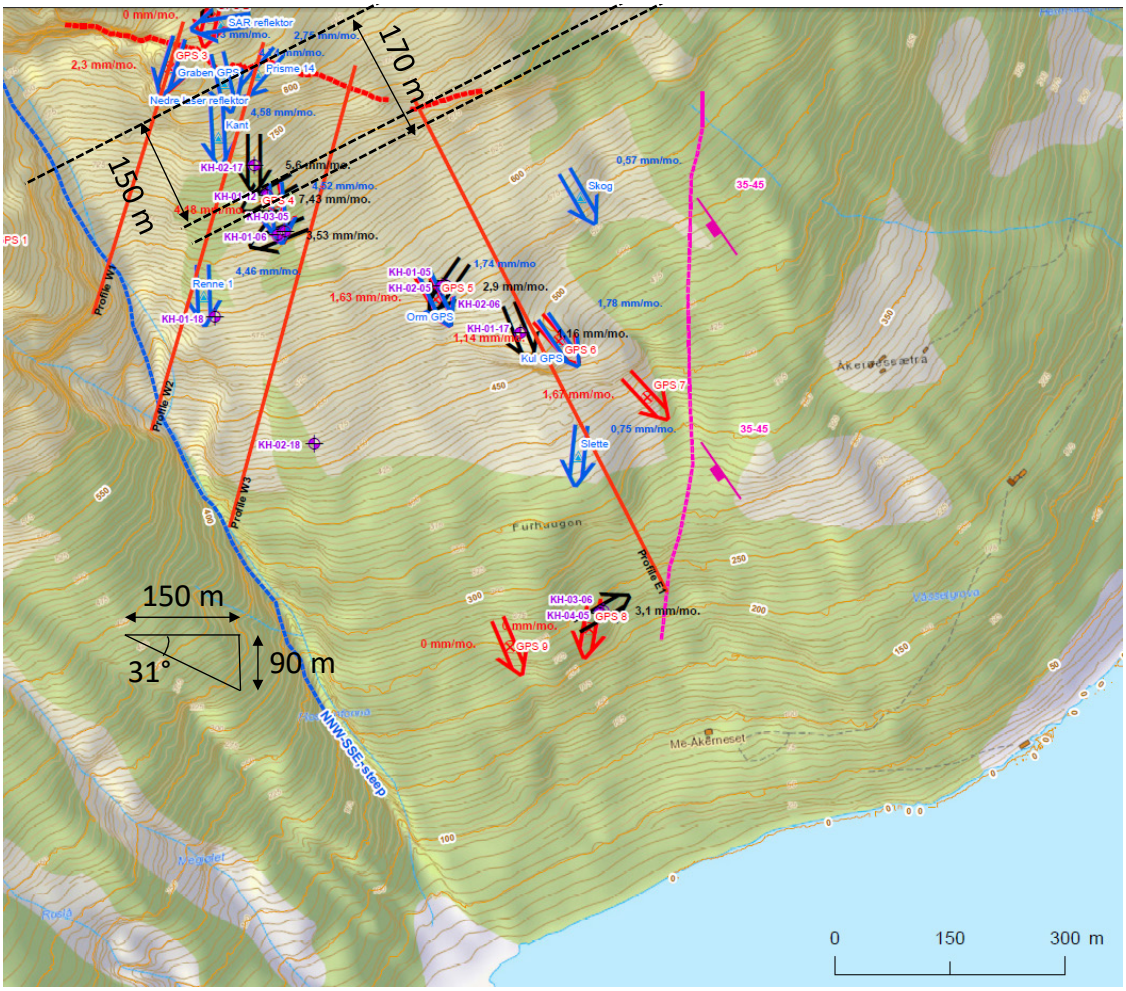

Figure 14 Calculating the vertical elevation changes of a joint belonging to the foliation parallel joint set (Table 3) between location cross-sections W2 and E1. The black dashed lines show the strike of the joint at different locations.

Frei (2008) carried out extensive tracer tests in Åknes to understand the groundwater system. Assuming hydrostatic condition, meaning that the groundwater velocity is neglectable, he developed equipotential lines for the places observing trace material flowing out (Figure 15). The equipotential lines from Figure 16 were compared with the numerical results for cross-sections of W2 and E1. The cross-sections were added to Figure 16 and the locations where waterhead was compared with the numerical results were marked by green ovals. Figure 17 shows the ground surface level of the ovals in Figure 16 (blue lines) and corresponding groundwater table (red lines). As this compression shows the calculated water head in the numerical models are coinciding well with suggested water table by Frei (2008).

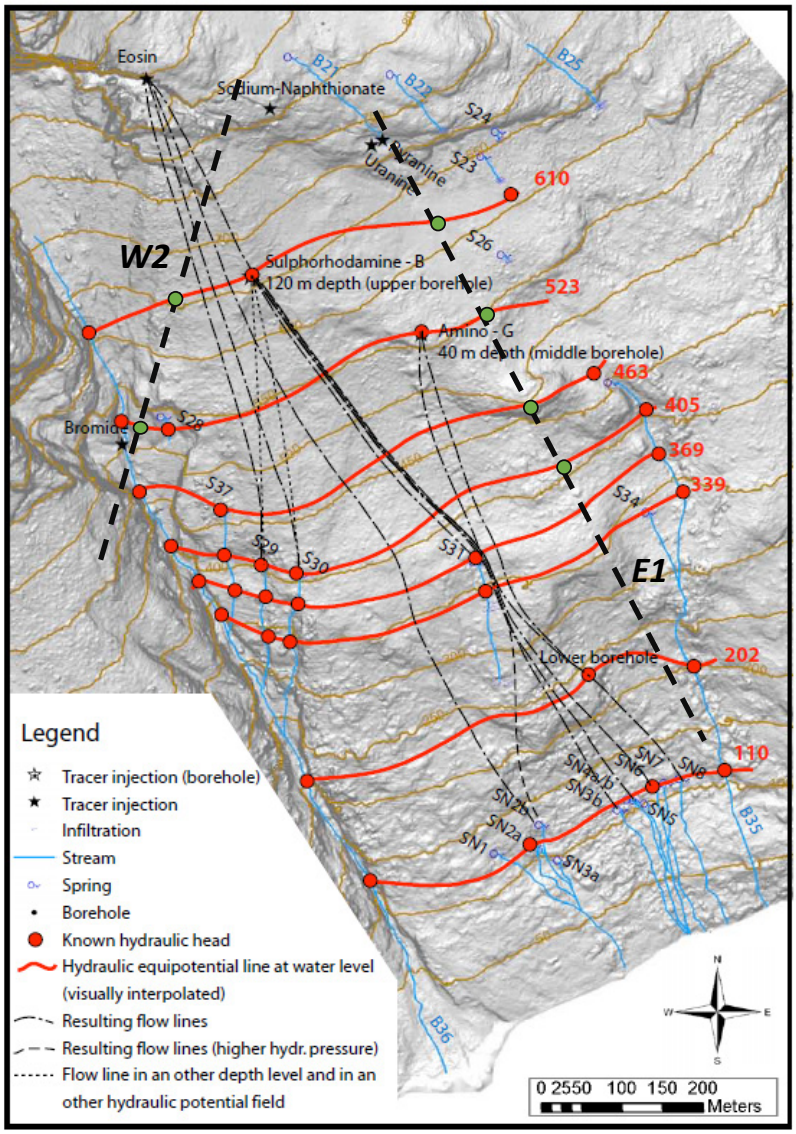

- ***Points where groundwater table was compared with numerical models***

Figure 15 Conceptual hydrostatic potential field of groundwater showing the equipotential lines representing the ground water table (water head = 0). Cross-section lines of W2 and E1 is added to the figure and the points (green dots) at which the groundwater level obtained by numerical models is compared. (After Frei 2008 [17]).

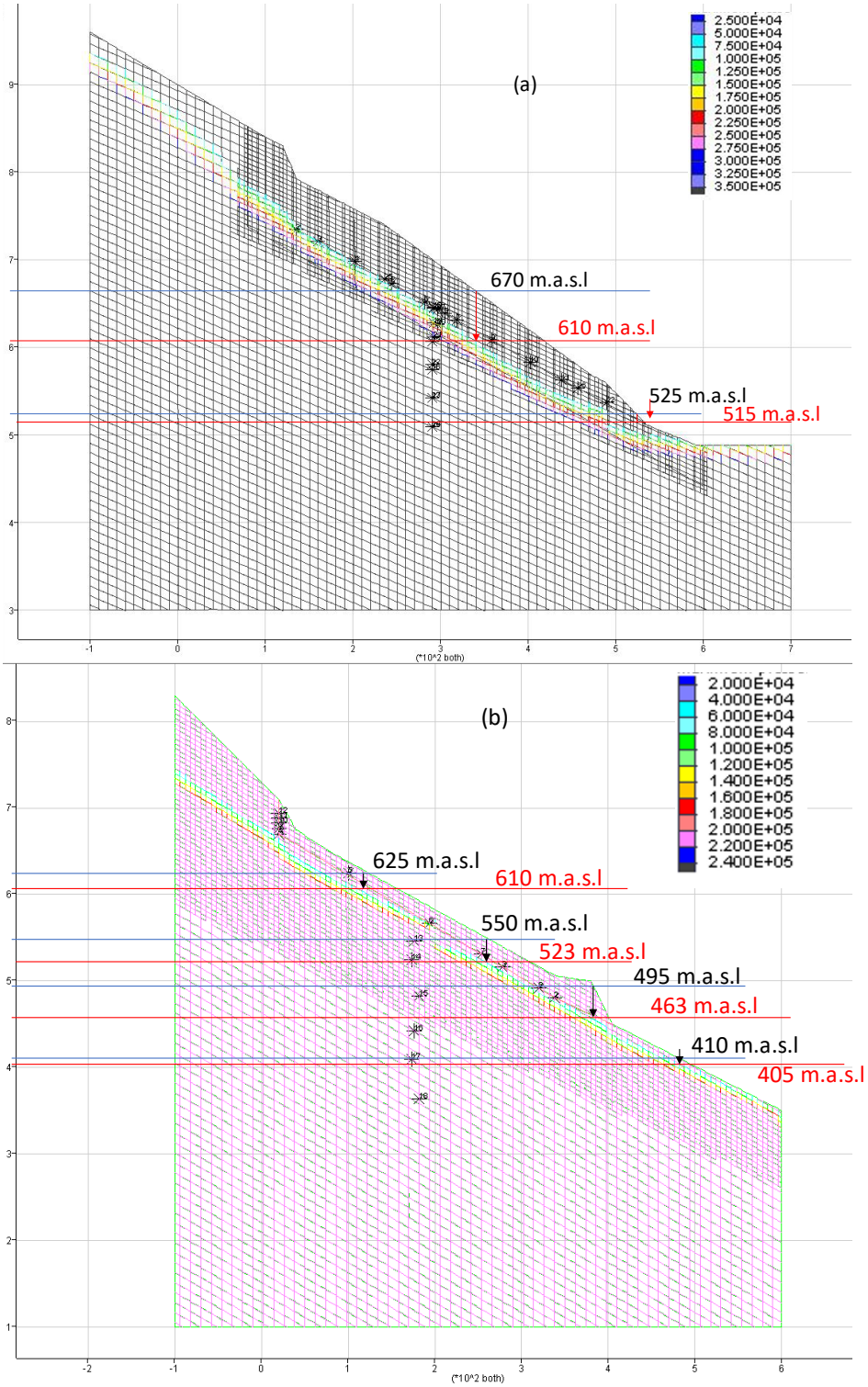

Figure 16 Observed groundwater level in the marked points in Figure 15. (a) cross-section W2 and (b) cross-section E1. Blue and red lines are representing the ground surface and water table elevations of the marked points.

5.2 Shearing resistance of the sliding plane in west and east flanks

For west and east flanks at the current condition, back calculated friction angle is equal to 32 and 27 degrees, respectively.

This difference can be explained as in KH-01-2017 (on cross-section E1) the sliding plane is a zone with thickness of ca. 1 m consisting of several crushed sections with clay. While in KH-02-2017 (representing cross-section W2) the sliding plane is only 10 – 20 cm of crushed rock with clay. Therefore, it might be expected to encounter a lower friction angle in the east side than west side.

However, the velocity of sliding in the west flank is larger than in the east flank. This can be explained by the Physics law of motion. As we know based on today's condition, the slope in both west and east flanks have approximately constant velocity, that means constant acceleration approximately equal to zero. Therefore, we can use the motion equations for constant acceleration [20] to check the sliding velocity in both cross-sections:

$$V^2 - V_0^2 = 2aZ \qquad \text{(Eq. 8)}$$

Where
V: current velocity of the moving mass
V_0: initial velocity which is equal to zero in our case
a: acceleration; which is very small value and equal for both east and west flank
Z: elevation changes in gravity centre of moving mass

We can rewrite the equation above as:

$$V = \sqrt{2aZ} \qquad \text{(Eq. 9)}$$

In west flank, the sliding surface has slightly larger dip angle (32 degrees) compared to east flank (27 degrees). Therefore, during the same time period, the elevation of the gravity centre of the moving mass in the west side has moved more than the east side ($Z_W > Z_E$). As a result, the velocity in the west side should be larger than the east side. In addition, the total displacement in the west flank should be larger than east flank; which can be confirmed with the opening of the backscarp is larger in the west flank than east flank and ongoing monitoring.

5.3 Different water head scenarios and their effect on the stability of Åknes slope

Two different scenarios were analysed in this chapter:

- Rapidly filling the backscarp with water due to flooding.
- Groundwater head rising to its theoretical highest value in the higher elevations above the backscarp. In the other words, the water table reaches to the ground surface at elevations higher than the backscarp.

5.3.1 Rapidly filling of backscarp

Since the rock mass permeability is in order of 1E-6 m/s; it takes time (from several hours to days) for the water to flow inside the rock mass. Therefore, it might be probable that during flooding at the ground surface (due to heavy rain or fast snow melting) the backscarp will totally be filled with water. During this situation, the water collected inside the backscarp will not dissipate simultaneously with infilling which will lead to excessive loading on the unstable mass. This situation is investigated below for the west flank.

For this analysis the following assumptions have been made:

- The backscarp is fully developed and connects to the sliding plane.
- The backscarp is open and it is possible to be rapidly filled with water flowing on the ground surface.
- The water flow inside of the rock mass is comparably slower than infilling the backscarp.

Åknes rock slope has shown a planar sliding mechanism which has formed a backscarp (Figure 17). Using analytical technique the driving force of the sliding mass can be obtained from:

$$F = wsin(\theta) + F_{bs}\cos(\theta) \quad \text{(Eq. 10)}$$

And resistance force, given cohesion equal to zero:

$$R = [wcos(\theta) - u - F_{bs}\sin(\theta)]\tan(\varphi) \quad \text{(Eq. 11)}$$

Where
w: weight of the moving mass
θ: dip angle of sliding surface
u: mean water uplift force on the sliding surface
φ: The friction angle of the sliding surface
F_{bc}: horizontal force generated by the water pressure filling the backscarp. Which can be determined by:

$$F_{bs} = \frac{\gamma_w h^2}{2} \quad \text{(Eq. 12)}$$

Where
γ_w: unit weight of water (0.01 MN/m^3)
h: height of water filled the backscarp

The factor of safety for the sliding mass can be calculated as:

$$FOS = \frac{R}{F} \quad \text{(Eq. 13)}$$

It should be noted that by using formulas 10-12 for a 2D cross-section, then all the forces will be per meter slope seen along the strike direction of the slope.

In order to control the calculations, first formulas 10-13 were used for back-calculation of the frictional resistance of the sliding plane in cross-section W2 (Table 6). The results of the analysis are presented in Table 8.

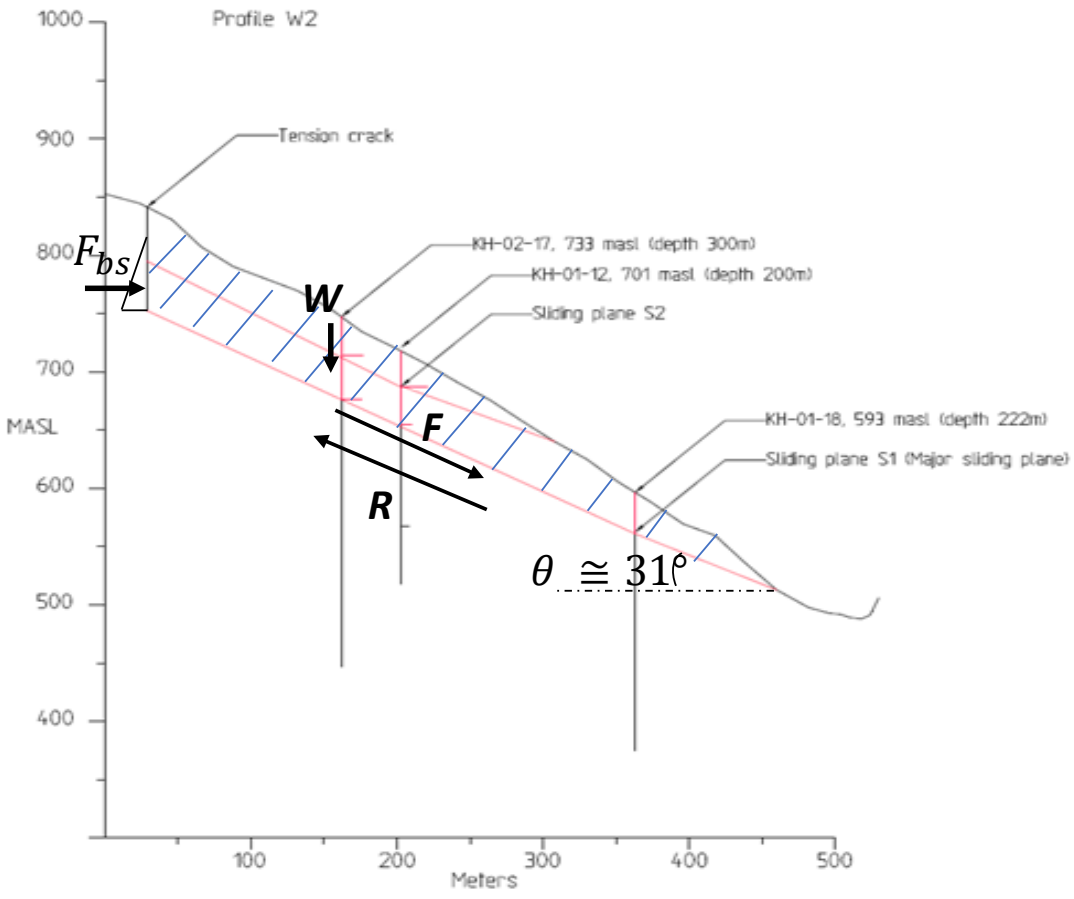

Figure 17 Free diagram of moving mass in cross-section W2.

Table 8 Back-calculated frictional resistance of the cross-section W2 using analytical technique.

Parameter	Unite	Value	Comment
Weight, w	MN/m of slope	625.59	Calculated area from CAD file multiplied by density of rock mass (0.027 MN/m^3)
u	MN/m	21.57	Mean water pressure on the sliding plane obtained by numerical modelling, Figure 11. In case normalising it to the length of the sliding plane a mean water pressure of 4.2 m of water will stand on the sliding surface.
h	m	17.5	From UDEC modelling
F	MN/m	323.51	From Eq. 10
θ	Degrees	31	-
ϕ	Degrees	32	-
R	MN/m	321.11	From Eq. 11
FOS	-	0.99	From Eq. 13

Now, assuming that the water fills totally the backscarp while the groundwater head at the sliding surface is same as before as presented in Table 8 (u = 21.57 MN/m), it leads to factor of safety equal to 0.89 (Table 9).

Table 9 Calculating FOS for cross-section W2 when the backscarp is fully filled with water.

Parameter	Unite	Value	Comment
Weight	MN / m of slope	625.59	-
u	MN/m	21.57	-
h	m	80	-
F	MN/m	349.63	-
θ	Degrees	31	-
ϕ	Degrees	32	-
R	MN/m	311.3	-
FOS	-	0.89	-

5.3.2 Effect of highest hypothetical groundwater level on stability

Figure 18 presents a hypothetical case when the groundwater table reaches to the ground surface at higher elevation above the backscarp. This case is hypothetical, and it is higher than that the maximum possible level of water table in Åknes rock slide. Nevertheless, it can be considered as hypothetical worst-case scenario, which should not be used for decision making, but should be considered as sensitivity analysis studying the sliding mechanism.

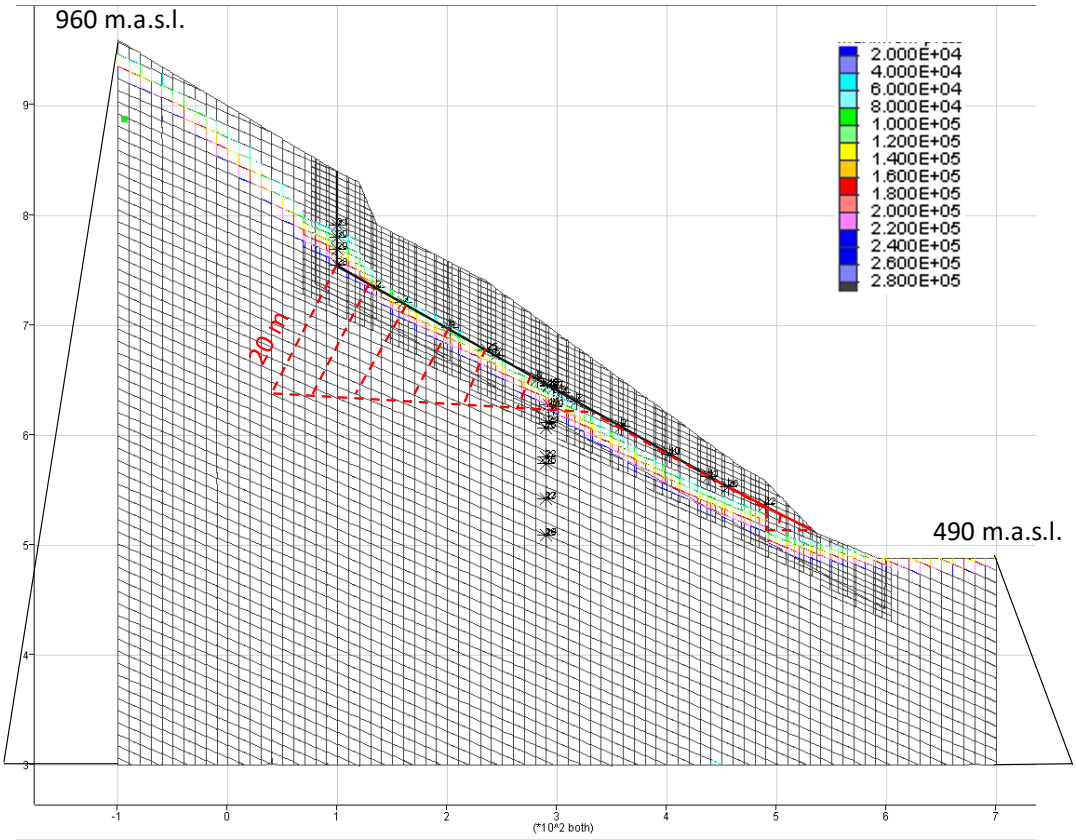

Figure 18 Numerical results of water pressure distribution inside the rock mass for worst case scenario (theoretically possible highest groundwater level). For visualisation purpose the maximum water pressure contour was limited to 28E4 Pa (28 m of water head).

Numerical modelling of cross-section W2 shows that groundwater rise does not change the major water transporting channels of the slope. Only the peak water pressure at the location of backscarp increased from 17.5 m to 20 m. This is due to a fact that the rock mass is already filled with water and there is very small room for extra increase in the groundwater head. In addition, well interconnected joint system helps the slope to be self-drained which regulates the water head and keeps the water head almost constant (See for example water head in borehole KH-01-2012 showing almost constant groundwater level in the borehole for several years [1]).

In this situation, assuming friction angle of 32 degrees for the sliding surface in W2 (back calculated for current condition of the slope) leads to factor of safety equal to 0.74. Meaning that the slope will be unstable, if such scenario should happen.

As demonstrated in chapter 5.1 due to the topography and dipping direction of the foliation parallel joint set, which is the main water transporting channel, groundwater level in the east side should be lower compared to the west side (as it was calculated in chapter 5.1; it should be ca. 90 m lower). Doing same calculations for the water head for the far east point of the backscarp (located at elevation of 700 m.a.s.l., see Figure 14)

shows that the water head in the east end of the backscarp should be ca. 102 m at lower elevation compare to cross-section W2.

As demonstrated in Chapter 4 for the current condition, the groundwater table at the backscarp is located at elevation of 780 m.a.s.l in cross-sectionW2. Deducting 102 m leads to that the groundwater head at the end of the backscarp in the far east point should be at elevation of ca. 678 m.a.s.l. An interesting observation at the site is that there is visible spring at this level (Figure 19).

In the worst-case scenario ground water can rise until 790 m.a.s.l in the backscarp of the cross-section W2. Using same analogy, the groundwater table should stand at elevation of 700 and 688 m.a.s.l at the backscarp in cross-section E1 and the far east point of the backscarp, respectively.

Worst-case scenario of the groundwater similarly to cross-section W2 was simulated for cross-section E1 (Figure 20). It shows that after rising the groundwater to the hypothetical extreme condition, approximately constant groundwater head develops on the surface of the sliding plane (ca. 10 m) in a limited area. In this situation, factor of safety with using friction angle of 27 degrees decrease from 1.00 (at the current condition) to 0.94. It is visible also that the groundwater head at the backscarp is at elevation of 700 m.a.s.l as demonstrated theoretically above.

In a hypothetical extreme scenario for groundwater head; the factor of safety in cross-sections W2 and E1 decrease to 0.74 and 0.94, respectively. Since the ground water flows from northwest towards southeast the groundwater rise will affect the west flank first. Therefore, it is most likely that in a worst-case scenario of groundwater rise, the west flank will become unstable first. If a landslide occurs in the west flank this can release the groundwater pressure and the east flank may become stable.

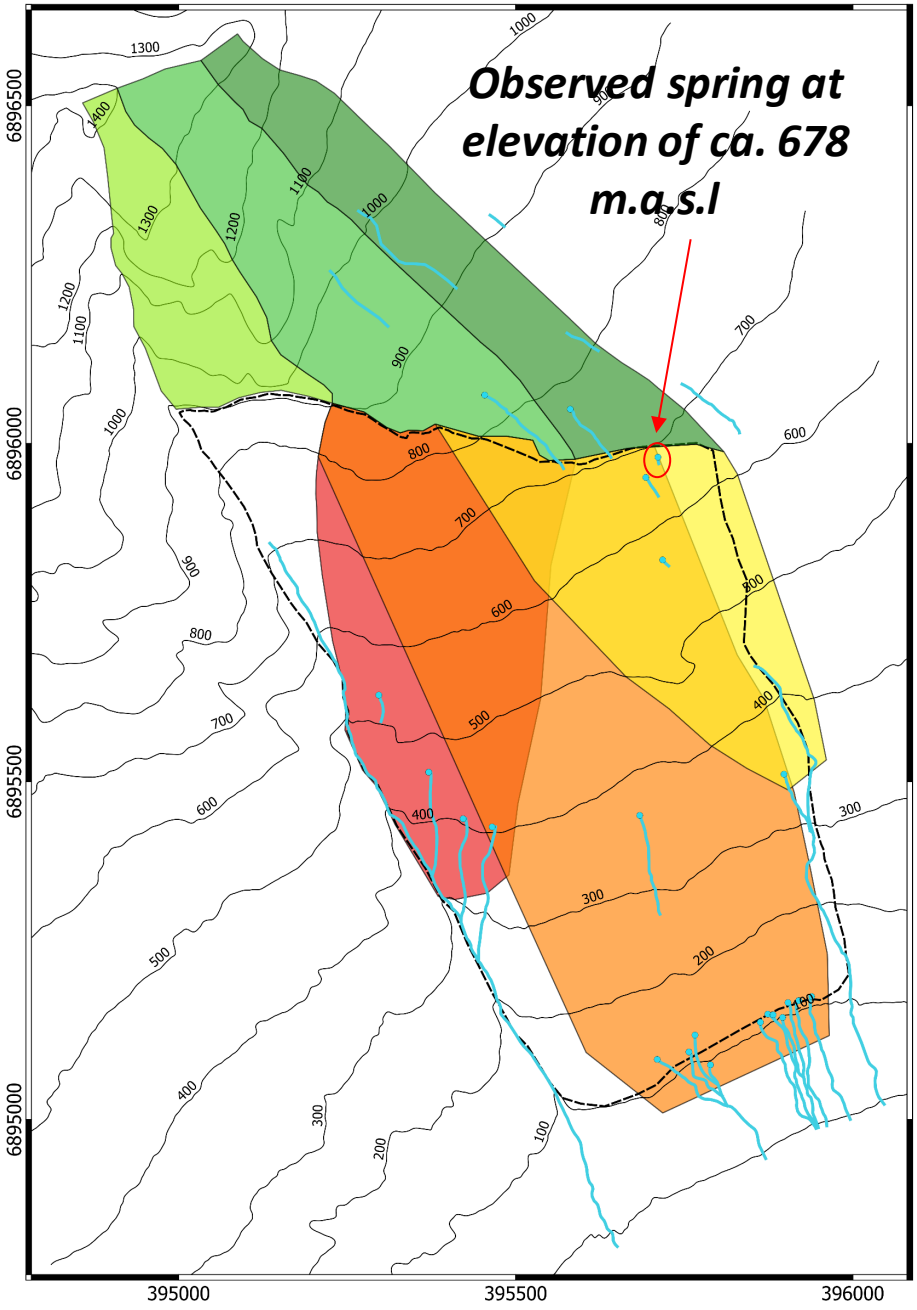

Figure 19 Observed springs at elevation 678 m.a.s.l. as predicted by the reverse calculations from the water level numerically obtained in the backscarp of cross-section W2. Modified from Clara Sena's figure presented November 2019.

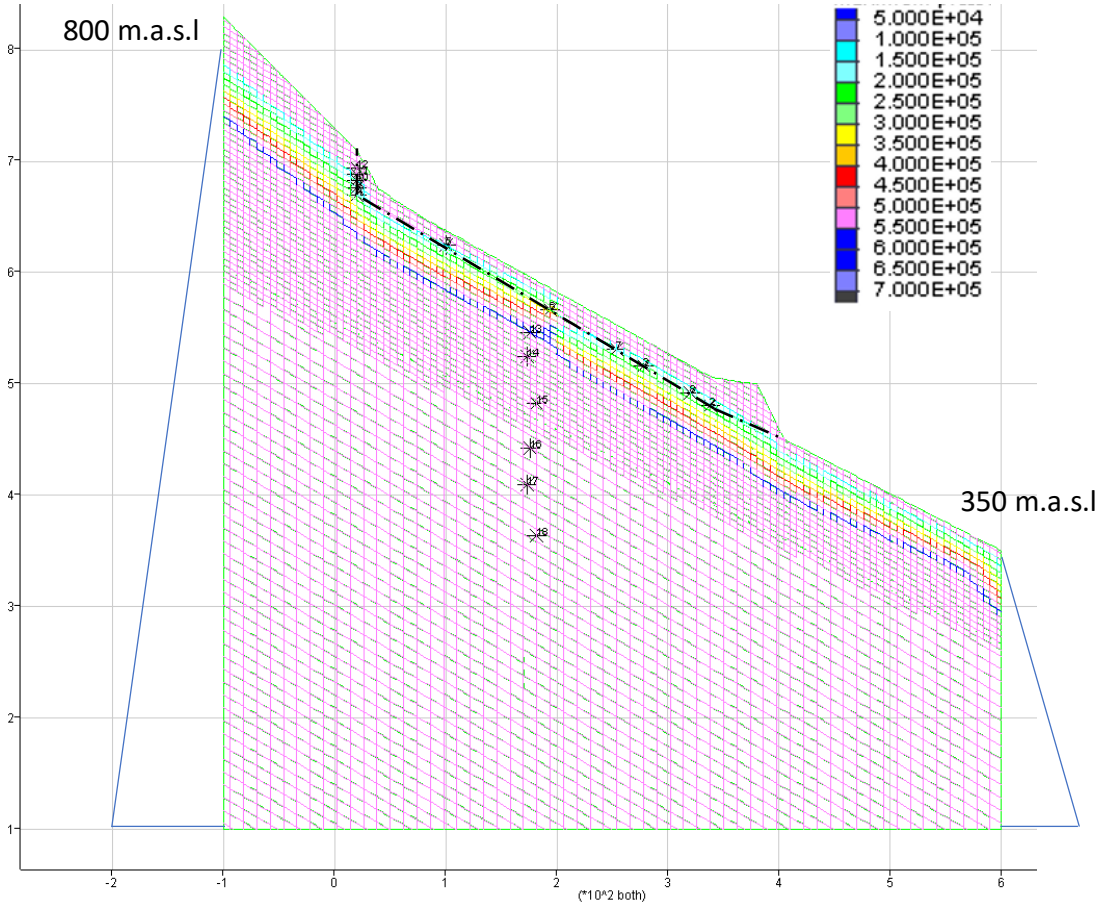

Figure 20 Numerical results of water pressure distribution inside the rock mass for worst case scenario (theoretically possible highest groundwater level). For visualisation purpose the maximum water pressure contour was limited to 70E4 Pa (70 m of water head).

6 Conclusions and suggestions

- Drainage of the groundwater will improve factor of safety 0.5 – 4 percent, in case of 100% effective drainage (zero water pressure on the sliding plane).

- Rapidly filling of the backscarp with water due to flooding at the ground surface (after a heavy rain or extreme snow melting) can make the slope unstable; decreasing factor of safety from 1.00 to 0.89 in the west flank.

- Considering a hypothetical condition for the groundwater which represents highest groundwater head on the sliding plane; it was shown that the factor of safety will decrease to 0.74 and 0.94 in west and east flank, respectively. Under such conditions, considering the groundwater flow direction, the west flank will become unstable earlier than east flank. Sliding failure of the west flank may dissipate the excessive groundwater pressure leading the east flank to remain

stable. This conclusion needs to be verified further by 3D coupled hydro-mechanical modelling.

- Through a 3D coupled hydromechanical model the highest possible water head in the sliding mass can be assessed. This analysis should include the entire Åknes mountainside including Instevatn, rainfall and existing groundwater deposited inside the rock mass.

7 References

[1] NGI. Åknes rock slope. Hydrogeological report. (2020), RN: 20180662-06-R.

[2] NGI, Åknes rock slide: Monitoring and displacements. 2020, RN: 20180662-05-R.

[3] NGI, Stabilitetsvurdering omkring Remnane ved Åkernes i Stranda, 1989, RN: 85494-2.

[4] Barton N, Bandis S, Bakhtar K. Strength, deformation and conductivity coupling of rock joints. Int. J. Roc. Mech. Min. Sci. & Geomech. Abstr. Vol. 22(03); pp: 121-140, 1985.

[5] NGI. Åknes landslide: Numerical simulation of the Åknes landslide using universal distinct element codes (UDEC). 1996, RN: 585910-4.

[6] Kveldsvik V, Einstein HH, Nilsen B, Blikra LH. Numerical analysis of the 650,000 m2 Åknes rock slope based on Measured displacements and geotechnical data. Rock Mech Rock Eng (2009); 42:689-728.

[7] Kveldsvik V, Keynia AM, Nadim F, Bhasin R, Nilsen B, Einstein HH. Dynamic distinct-element analysis of the 800 m high Åknes rock slope. Int. J Rock Mech & Min Sci (2009); 46: 686 – 689.

[8] Grøneng G, Nilsen B, Sandven R. Shear strength estimation for Åknes sliding area in western Norway. Int. J Rock Mech & Min Sci (2009); 46: 479 – 488.

[9] Grøneng G, Lu M, Nilsen B, Jenssen AJ. Modelling of time-dependent behaviour of the basal sliding surface of the Åknes rockslide area in western Norway. Engineering Geology (2010); 114: 414 – 422.

[10] Langeland H (2014). Utvikling av revidert geologisk modell og stabilitetsanalyser for øvre deler av ustabil fjellside på Åknes. M.Sc. Thesis, NTNU.

[11] Grøneng G (2010). Stability analyses of the Åknes rock slope, western Norway. Ph.D Thesis, NTNU.

[12] Tønset L (2019). Verdien av kjerneborehull for økt forståelse av stabilitetsforhold ved Åknes skredområdet. M.Sc. Thesis, NTNU.

[13] Kveldsvik V (2008). Static and dynamic stability analysis of the 800 m high Åknes rock slope, western Norway. Ph.D Thesis, NTNU.

[14] Kveldsvik V, Nilsen B, Eintein H H, Nadim F. Alternative approaches for analyses of a 100,000 m^3 rock slide based on Barton-Bandis shear strength criterion. Landslides (2007) 1-16

[15] Ganerød GV, Grøneng G, Rønning JS, Dalsegg E, et al. Geological model for the Åknes rockslide, western Norway. Engineering geology (2008); 102: 1-18.

[16] Ringstad SRS (2019). The influence of structural discontinuities on the stability of the Åknes rockslide. M.Sc. Thesis, Oslo University.

[17] Frei C (2008). Groundwater flow at the Åknes Rockslide site (Norway). M.Sc. thesis, Swiss Federal Institute of Technology Zurich (ETH).

[18] Barton N, Choubey V. The shear strength of rock joints in theory and practice. Rock Mech. 10, 1-54. (1977).

[19] Itasca (2014), Universal Distinct Element Code – UDEC manual, V 6.0.

[20] Meriam JL, Kraige LG(2012). Engineering Mechanics: Dynamics. 7^{th} edition, Wiley, USA.

[21] Barton N (1972). Suggested methods for Quantitative Description of Discontinuities in Rock Masses. ISRM suggested methods, Pergamon Press.

Kontroll- og referanseside/ Review and reference page

Dokumentinformasjon/*Document information*		
Coupled hydro-mechanical stability analysis of Åknes rock slope		**Dokumentnr./*Document no.*** 20180662-07-R
Dokumenttype/*Type of document* Rapport / Report	**Oppdragsgiver/*Client*** NVE	**Dato/*Date*** 2020-12-18
Rettigheter til dokumentet iht kontrakt/ *Proprietary rights to the document according to contract* Oppdragsgiver / Client		**Rev.nr.&dato/*Rev.no.&date*** 0
Distribusjon/*Distribution* BEGRENSET: Distribueres til oppdragsgiver og er tilgjengelig for NGIs ansatte / LIMITED: Distributed to client and available for NGI employees		
Emneord/*Keywords* Åknes, Rock slope, Numerical modelling, Stability analysis, Drainage		

Stedfesting/*Geographical information*	
Land, fylke/*Country* Norway	**Havområde/*Offshore area***
Kommune/*Municipality* Stranda	**Feltnavn/*Field name***
Sted/*Location* Åknes	**Sted/*Location***
Kartblad/*Map* Geiranger 1219 II	**Felt, blokknr./*Field, Block No.***
UTM-koordinater/*UTM-coordinates* **Zone: East: North:** UTM32 X 395170 Y 6891861	**Koordinater/*Coordinates*** **Projection, datum: East: North:**

Dokumentkontroll/*Document control*
Kvalitetssikring i henhold til/*Quality assurance according to NS-EN ISO9001*

Rev/ *Rev.*	**Revisjonsgrunnlag/*Reason for revision***	**Egenkontroll av/ *Self review by:***	**Sidemanns-kontroll av/ *Colleague review by:***	**Uavhengig kontroll av/ *Independent review by*:**	**Tverrfaglig kontroll av/ *Interdisciplinary review by:***
0	Original document	2020-12-10 Mahdi Shabanimashcool	2020-12-16 Vidar Kveldsvik		

Dokument godkjent for utsendelse/ *Document approved for release*	**Dato/*Date***	**Prosjektleder/*Project Manager***
	18 December 2020	Kristin H. Holmøy

NGI (Norwegian Geotechnical Institute) is a leading international centre for research and consulting within the geosciences. NGI develops optimum solutions for society and offers expertise on the behaviour of soil, rock and snow and their interaction with the natural and built environment.

NGI works within the following sectors: Offshore energy – Building, Construction and Transportation – Natural Hazards – Environmental Engineering.

NGI is a private foundation with office and laboratories in Oslo, a branch office in Trondheim and daughter companies in Houston, Texas, USA and in Perth, Western Australia

NGI (Norges Geotekniske Institutt) er et internasjonalt ledende senter for forskning og rådgivning innen ingeniørrelaterte geofag. Vi tilbyr ekspertise om jord, berg og snø og deres påvirkning på miljøet, konstruksjoner og anlegg, og hvordan jord og berg kan benyttes som byggegrunn og byggemateriale.

Vi arbeider i følgende markeder: Offshore energi – Bygg, anlegg og samferdsel – Naturfare – Miljøteknologi.

NGI er en privat næringsdrivende stiftelse med kontor og laboratorier i Oslo, avdelingskontor i Trondheim og datterselskaper i Houston, Texas, USA og i Perth, Western Australia.

www.ngi.no

NGI
OSLO
TRONDHEIM
HOUSTON
PERTH

NORWEGIAN GEOTECHNICAL INSTITUTE
NGI.NO

Main office
PO Box 3930 Ullevaal St.
NO-0806 Oslo
Norway

Trondheim office
PO Box 5687 Torgarden
NO-7485 Trondheim
Norway

T (+47)22 02 30 00
F (+47)22 23 04 48
NGI@ngi.no

BIC NO. DNBANOKK
IBAN NO26 5096 0501 281
ORGANISATION NO.
958 254 318MVA

ISO 9001/14001
CERTIFIED BY BSI
FS 32989/EMS 612006